Review

# Effects of carbon dioxide on laminar burning speed and flame instability of methane/air and propane/air mixtures: A literature review

Ziyu Wang, Sai Chandra Yelishala, Guangying Yu, Hameed Metghalchi, and Yiannis Angelo Levendis

*Energy Fuels*, **Just Accepted Manuscript** • DOI: 10.1021/acs.energyfuels.9b02346 • Publication Date (Web): 20 Sep 2019

# Effects of carbon dioxide on laminar burning speed and flame instability of methane/air and propane/air mixtures: A literature review

Ziyu Wang*, Sai C Yelishala, Guangying Yu, Hameed Metghalchi, Yiannis A. Levendis

*Department of Mechanical and Industrial Engineering, Northeastern University, Boston, MA 02115, USA*

## Abstract

This article reviews the impact of carbon dioxide ($CO_2$) on laminar burning speed and stability of the flame for methane ($CH_4$) and propane ($C_3H_8$) combustion with air. Mixtures of $CH_4$ and $CO_2$, also known as biogas, are considered as low-cost alternative fuels. Biogas is widely used in various industrial and residential applications. Mixtures of $C_3H_8$ and $CO_2$ are considered as alternative refrigerants with low global warming potential and low flammability. Laminar burning speeds were reported using different experimental methods. Laminar burning speeds have also been numerically calculated by one-dimensional steady code using three chemical kinetic mechanisms. Results depict a decrease in equilibrium flame temperature and laminar burning speed of both $CH_4$/air and $C_3H_8$/air mixtures with the existence of $CO_2$ in those mixtures. The maximum laminar burning speeds of neat $CH_4$ and $C_3H_8$ are observed to be in the vicinity of an equivalence ratio of 1.1; however, as the percentage of $CO_2$ increases the maximum laminar burning speeds shift toward stoichiometric mixtures. Carbon dioxide also increases flame thickness and suppresses flame instability by the combination of thermal-diffusive and hydrodynamic effects.

Keywords: laminar burning speed, flame instability, carbon dioxide, methane, propane

## 1. Introduction

Biogas is primarily a mixture of $CH_4$ and $CO_2$. It may also contain small amounts of water vapor, siloxane, hydrogen sulfide, carbon monoxide, oxygen, nitrogen, hydrogen, and ammonia. Biogas is obtained either by anaerobic digestion with methanogen or anaerobic organisms that digest organic material in a reactor or by fermentation of biodegradable materials [1]. Biogas is a low-cost alternative fuel, which is used in gas turbines, internal combustion engines, cooking, and heating applications [2]. However, research on biogas in internal combustion engines shows that the existence of $CO_2$ in the mixture decreases thermal efficiency, increases unburned hydrocarbon emissions, and reduces thermal $NO_X$ emissions when compared to natural gas [3–7].

Propane and other liquefied petroleum gases (LPG) have been used in various industrial and residential applications, in a manner similar to biogas [8]. Research shows that comparing to conventional fuel $C_3H_8$ has lower CO and $NO_X$ emissions in engine applications [9]. Also, products of combustion of propane and methane have lower greenhouse gas emissions than most other fossil fuels, like gasoline and diesel oil, due to

*Corresponding Author Email: wang.ziyu2@husky.neu.edu

its lower carbon content. The addition of $CO_2$ into the fuel mixture lowers the flame temperature, which can reduce thermal $NO_X$ emissions [10, 11].

Propane has also been considered as an alternative refrigerant in heating, ventilation, and air conditioning (HVAC) applications as it is a natural and environmentally friendly refrigerant [12]. However, its high flammability limits its extensive usage because of fire safety concerns. By blending $CO_2$ with $C_3H_8$, the mixtures can be classified as low flammability refrigerants [13].

It is crucial to study vital combustion properties like laminar burning speed and stability of the flame for $CH_4/CO_2$/air and $C_3H_8/CO_2$/air mixtures, to understand how they perform over various operating conditions. Laminar burning speed adequately describes the essential characteristics of the fuel/oxidizer mixtures regarding thermal diffusivity, exothermicity, and reactivity. It is essential in calculating turbulent burning speed and validating chemical kinetic mechanisms. Flame instability describes the flame transition from smooth to cellular, which is an essential characteristic of fuel/oxidizer mixtures. Two significant contributors to flame instability are hydrodynamic effects and thermal-diffusive effects [7, 12].

This article presents a thorough study on the literature of the laminar burning speed for $CH_4/CO_2$/air & $C_3H_8/CO_2$/air blends and investigates the effects of $CO_2$ on laminar burning speed and the stability of the flame for varying $CO_2$ concentrations, equivalence ratios, temperatures, and pressures.

Methane and Carbon Dioxide: Stone et al. [14] developed a correlation for laminar burning speed of $CH_4/CO_2$/air blends for $CO_2$ concentrations of 0–60%, pressures of 0.5–10.4 bar, temperatures of 295–494 K, and equivalence ratios of 0.6–1.4. They measured pressure as a function of time to calculate laminar burning speed in a spherical constant volume vessel. Hinton and Stone [15] later expanded their correlation to incorporate high temperatures till 520 K. Kishore et al. [16] measured laminar burning speed of natural gas by a heat flux method and studied the effects of $CO_2$ (0–60%) on flame properties at equivalence ratios (0.6–1.4), temperature of 307 K and atmospheric pressure. Vital flame properties of hydrocarbons ($C_1$–$C_4$)/$CO_2$ mixtures were investigated by Park et al. [17] experimentally and numerically. They used counterflow flame method to determine laminar burning speeds, ignition limits and extinction limits of premixed flames at pressures of 1, 2, 4 atm and atmospheric temperature. Xie et al. [18] investigated flame properties of biogas/oxygen mixtures experimentally and numerically. They measured laminar burning speeds by using a spherical flame at equivalence ratios (0.4–1.6), temperature of 298 K, and pressures (0.1–0.3 MPa). They also investigated the influence of $CO_2$ on the sensitivity of chemical reactions, flame radiation, and the stability of the flame. Cardona et al. [19] measured laminar burning speed for biogas/air blends in a contoured slot burner at a pressure of 0.828 atm & atmospheric temperature. Zahedi and Yousefi [20] conducted experimental and numerical studies on the influence of $CO_2$ on $NO_x$ formation and the laminar burning speed for $CH_4$/air mixtures at equivalence ratios (0.7–1.3), pressures (0.1–0.5 MPa), and a temperature of 298 K. Chan et al. [21] measured laminar burning speed for $CH_4/CO_2$/air

blends utilizing flat flame burner at standard conditions for a range of equivalence ratios (0.8–1.4). Nonaka and Pereira [22] measured laminar burning speed of biogas experimentally & calculated numerically for varying $CO_2$ concentrations (0%–50%) at atmospheric temperature and pressure. Their numerical results showed that thermal and reaction effects caused the shifting of maximum laminar burning speed to leaner mixtures. Hu and Yu [23,24] investigated the influence of elevated temperatures (300, 400, & 543 K) on laminar burning speed for biogas oxygen mixtures. Also, they studied the chemical and radiative effects of $CO_2$ on those mixtures. Bai et al. [7] burned $CH_4/CO_2$/air mixtures, and also developed power-law correlations for laminar burning speed of these mixtures for equivalence ratios (0.8–1.2), $CO_2$ concentrations (0%–60%), pressures (0.5–6.9 atm), and temperatures (298–661 K). They also studied the influence of $CO_2$ on flame instability. All the aforementioned studies of laminar burning speed for $CH_4/CO_2$/air blends are summarized in Table 1.

Propane and Carbon Dioxide: Akram et al. [25] measured laminar burning speed for $C_3H_8/CO_2$/air and $C_3H_8/N_2$/air blends. They conducted experiments using a preheated mesoscale diverging channel for equivalence ratios (0.7–1.3) and temperatures (370−650 K). Nair et al. [11] examined the influence of $CO_2$ and $N_2$ on the laminar burning speed for different liquid petroleum gases and air mixtures. They developed a power-law correlation for temperatures (300−500 K), equivalence ratios (0.8–1.3), and $CO_2$ percentages (0%–30%). Goswami et al. [26] measured laminar burning speed for $C_3H_8$/air mixture experimentally and studied numerically for equivalence ratios (0.8–1.3), pressures (1–4 atm), and atmospheric temperature. Yelishala et al. [12] conducted a constant volume experiment to measure laminar burning speed of $C_3H_8/CO_2$/air blends for equivalence ratios (0.7–1.2), $CO_2$ concentrations (0%–80%), pressures (0.5–6.2 atm), and temperatures (298–420 K). They studied flame stability using a Z-shaped Schlieren system by taking pictures during flame propagation. Fedyaeva et al. [27] examined the influence of $H_2O$ and $CO_2$ as diluents on $C_3H_8$ oxidation numerically at different pressures. All the aforementioned studies of laminar burning speed for $C_3H_8/CO_2$/air mixtures are summarized in Table 2.

Table 1. Literature studies on experimental laminar burning speed of $CH_4/CO_2$/air blends

| Ref. | Mixture | Pressure | Temperature | Equivalence Ratio | Experimental Method |
|---|---|---|---|---|---|
| [14] | 0-60% $CO_2$ | 0.5-10.4 bar | 295-454 K | 0.6-1.4 | Spherical constant volume |
| [16] | 0-60% $CO_2$ | 1 bar | 307 K | 0.8-1.3 | Flat flame burner (heat flux) |
| [17] | 25%, 45% $CO_2$ | 1, 2, 4 atm | 298 K | 0.75-1.25 | Counterflow Stagnation twin flame opposed jet configuration |
| [18] | $CH_4/O_2/CO_2$ | 1-3 bar | 298 K | 0.4-1.6 | Spherical constant pressure |
| [19] | 34% $CO_2$ | 0.828 atm | 298 K | 0.9-1.2 | Contoured slot burner |
| [20] | 0-20% $CO_2$ | 1-5 bar | 298 K | 0.7-1.3 | Flat flame burner (heat flux) |
| [15] | 0-40% $CO_2$ | 1-8 bar | 380-520 K | 0.7-1.4 | Spherical constant volume |
| [21] | 0-15% $CO_2$ | 1 bar | 298 K | 0.8-1.4 | Flat flame burner (heat flux) |
| [22] | 0-50% $CO_2$ | 1 atm | 298 K | 0.7-1.4 | Flat flame burner (heat flux) |
| [23,24] | $CH_4/O_2/CO_2$ | 1 atm | 300, 400, 543 K | 0.6-1.4 | Bunsen burner |
| [7] | 0-60% $CO_2$ | 0.5-6.9 atm | 298-661 K | 0.8-1.2 | Spherical constant volume |

Table 2. Literature studies on experimental laminar burning speed of $C_3H_8/CO_2$/air blends

| Ref. | Mixture | Pressure | Temperature | Equivalence Ratio | Experimental Method |
|---|---|---|---|---|---|
| [25] | 0-40% $CO_2$ | 1 atm | 370-650 K | 0.7-1.3 | Externally preheated divergent mesoscale channel |
| [12] | 0-80% $CO_2$ | 0.5-6.2 atm | 298-420 K | 0.7-1.2 | Spherical constant volume |

## 2. Experimental Methodologies

Different experimental methods have been undertaken to study laminar burning speed of $CH_4/CO_2$/air and $C_3H_8/CO_2$/air such as flat flame burner [16, 20–22], Bunsen burner [23, 24], counterflow/stagnation flame [17], constant pressure spherical flame [18], and constant volume spherical flame [7, 12, 14, 15]. Egolfopoulos et al. [28] recently reviewed the advances and challenges of these different methods.

Botha and Spalding [29] determined the energy loss in heat interaction incurred to stabilize the flame on a flat flame burner to measure adiabatic laminar burning speed. de Goey and co-workers [30] later established a heat flux setup to stabilize the flame and to determine the adiabatic laminar burning speed. In this method, the temperature of the unburned mixture is increased using a heating jacket, which compensates for the energy loss to the environment. This method can get rid of the stretch effect of the flame, while it is limited to low burning speed and atmospheric pressure and temperature measurement. Fig. 1 (a) illustrates the schematic of a flat flame burner.

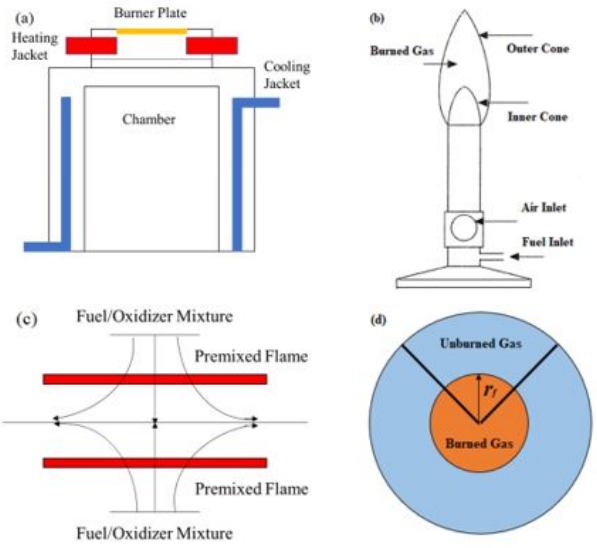


Fig. 1. Schematic of different experimental methods. (a) flat flame burner, (b) Bunsen burner, (c) counterflow/stagnation flame, (d) constant pressure or constant volume spherical flame.

Fig. 1 (b) shows the schematic of the Bunsen burner, which measures flame speed, $S_b$, for a conical flame where the reaction zone is assumed to have a 1–D flame speed, $S_b^0$ [23, 24]. Based on mass balance, the laminar burning speed, $S_u^0$, is calculated by

$$S_u^0 = \frac{\rho_b}{\rho_u} S_b^0 = \frac{\dot{m}}{\rho_u A_b} = \frac{\dot{Q}_u}{A_b} \quad (1)$$

where, $\dot{m}$ is mass flow rate, $\rho_b$ and $\rho_u$ are burned gas and unburned gases densities, and flame area, $A_b$, is obtained from the flame image. Volumetric flow rate, $\dot{Q}_u$, is determined by the mass flow controller (MFC). It is a simple method; however, the determination of flame area is complicated, and the stretch effect cannot be neglected.

Fig. 1 (c) shows the schematic of counterflow/stagnation flame experiments. There are two symmetric (twin) and planar flames with the same chemical composition in counterflow/stagnation flame configuration [31–33]. The axial velocity profile is determined by using laser Doppler velocimetry or particle image velocimetry. The maximum absolute value of flow velocity gradient is defined as the strain rate, $K$, and the minimum axial flow velocity is defined as the reference flame speed, $S_{u\,ref}$. $S_u^0$ is determined by extrapolation of $S_{u\,ref}$ to $K = 0$. Conductive energy loss of the flame is eliminated due to symmetry in this method, while it is challenging to create zero strain rate.

Fig. 1 (d) shows the schematic of spherical flames. The constant pressure method of spherical flames was first developed by Strauss and Edge [34] to measure laminar burning speed. Flame radius, $r_f$, varying with time, $t$, was captured using a Schlieren or shadowgraph system with a negligible pressure rise in the vessel. The burned gas speed is defined as

$$S_b = \frac{dr_f}{dt} \tag{2}$$

The stretch rate, $\kappa$ of the spherical flame is defined based on the flame surface area,

$$\kappa = \frac{d\ln A_b}{dt} = \frac{1}{A_b}\frac{dA_b}{dt} = \frac{2}{r_f}\frac{dr_f}{dt} \tag{3}$$

Subsequently, the zero-stretch burning speed related to burned gas, $S_b^0$, could be determined by linear or nonlinear extrapolation. Finally, $S_u^0$ is calculated through mass balance, $S_u^0 = \frac{\rho_b}{\rho_u} S_b^0$.

The constant volume method of spherical flames was first developed by Lewis and von Elbe [35] to measure pressure rise, $p$, in the vessel. The laminar burning speed is deduced using

$$S_u = \frac{dr_i}{dt}\left(\frac{r_i}{r_f}\right)^2 \left(\frac{p}{p_i}\right)^{\frac{1}{\gamma_u}} \tag{4}$$

where, $r_i$ is flame radius, $p_i$ is initial pressure, and $\gamma_u$ is ratio of specific heats for unburned gas.

Metghalchi, Keck, and co-workers [36–50] improved the laminar burning speed calculation using measured pressure rise in a constant volume vessel. They developed a multi-shell thermodynamic model and later modified it by considering effects of thermal boundary layer, preheat zone, burned gas temperature gradient, conductive and radiative energy losses.

They used the following equations for volume and energy to calculate the laminar burning speed

$$m\left[\int_0^{x_b} v_{bs}(T,p)dx + (1-x_b)v_{us}\right] = V_c - V_e + V_{eb} + V_{wb} + V_{ph} \tag{5}$$

$$m\left[\int_0^{x_b} e_{bs}(T,p)dx + (1-x_b)e_{us}\right] = E + \frac{pV_{ph}}{\gamma_u - 1} - A_{wb}\int_0^{\delta_{wb}} pd\delta - A_{eb}\int_0^{\delta_{eb}} pd\delta - Q_r \tag{6}$$

where $m$ and $E$ are total mass and energy, $x_b$ is mass fraction of burned gas, $v_{bs}$ and $v_{us}$ are specific volumes for burned and unburned mixtures; $V_c$ is chamber volume; $V_e$ is volume for electrodes; $V_{wb}$, $V_{eb}$, and $V_{ph}$ are displacement volumes for wall boundary layer; electrode boundary layer; and preheat zone; $e_{bs}$ and $e_{us}$ are specific energy of burned and unburned gases; $A_{wb}$ and $A_{eb}$ are areas of the wall and electrodes; $\delta_{wb}$ and $\delta_{eb}$ are displacement thicknesses for wall boundary layer and electrode boundary layer; and $Q_r$ is radiative energy loss.

For a given pressure, $p(t)$, two unknowns: mass fraction of burned gas, $x_b(t)$ and temperature of burned gas in the last shell, $T_b(r,t)$ can be solved by Eq. (5) and (6).

Finally, the laminar burning speed is calculated using

$$S_u = \frac{\dot{m}_b}{\rho_u A_b} = \frac{m\dot{x}_b}{\rho_u A_b} \quad (7)$$

where $\dot{x}_b$ is the mass fraction rate for burned gas.

Contrary to the constant pressure method of spherical flames that burning speed needs to be adjusted for stretch effects, constant volume method stretch effects are negligible because of high flame radius. This can be observed by analyzing Fig. 2 that shows laminar burning speeds of three different states. For each state, burning speed has been measured for 3-4 flame radii having different stretch rate. It shows that laminar burning speed becomes independent of stretch rate as long as $\kappa < 100$ s$^{-1}$. Therefore, in this study, only smooth (laminar) flames with $r_f > 4\ cm$, which have lower stretch rates, have been used.

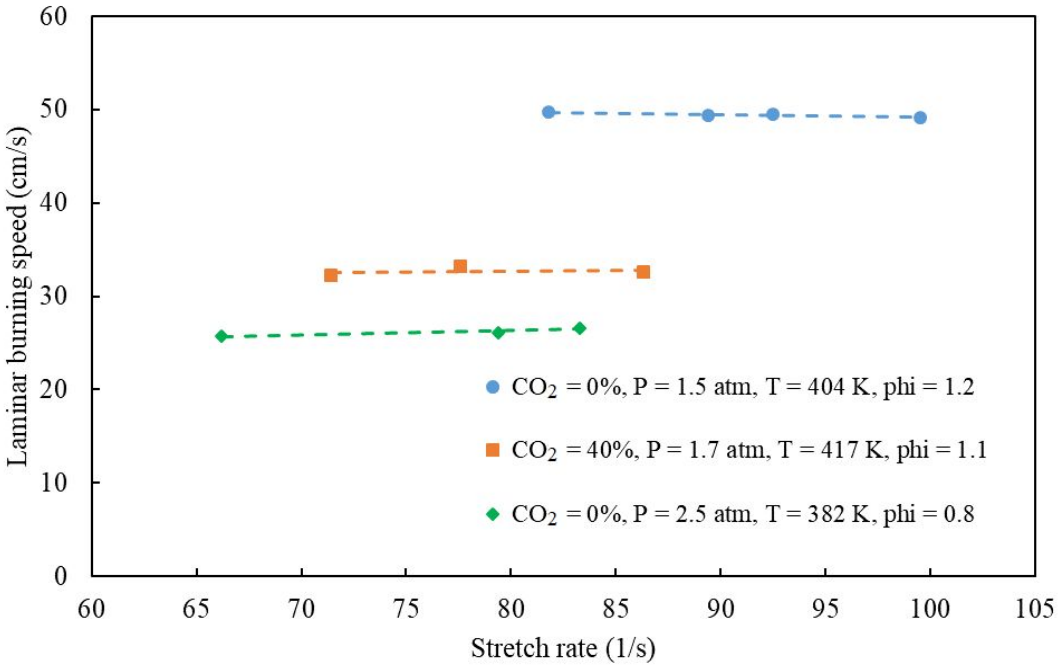


Fig. 2. Laminar burning speed of $CH_4$/air/$CO_2$ at different thermodynamic states with different stretch rates [7].

## 3. Effects of $CO_2$ on laminar burning speed

### 3.1. Methane/carbon dioxide/air mixture

Different experimental methods of laminar burning speed measurement in literature [7, 17, 20, 22, 51–56] were mentioned in Section 2. The experimentally measured laminar burning speeds and the numerical results calculated by 1–D steady state premixed flame code from CANTERA [57] are shown in this section. The numerical results were calculated using 3 chemical kinetic mechanisms: GRI-Mech 3.0 [58], USC Mech II [59], and San Diego [60]. The GRI-Mech 3.0 mechanism has 53 species and 325 chemical reactions and is adjusted to model methane combustion at pressures of 0.1–10 atm. The USC Mech II mechanism

has 111 species and 784 chemical reactions relevant to $C_1$–$C_4$ hydrocarbons and syngas oxidation at high temperature. The San Diego mechanism has 37 species and 177 chemical reactions and is optimized for auto-ignition and diffusive flames of different hydrocarbons [22]. Table 3 lists different numerical methods burning $CH_4/CO_2$/air blends in literature.

Table 3. Literature on numerical calculation of laminar burning speed for $CH_4/CO_2$/air blends

| Ref. | Mixture | Numerical Method |
|---|---|---|
| [16, 20] | $CH_4/CO_2$/air | CHEMKIN programs using GRI-Mech 3.0 mechanism |
| [17] | $CH_4/CO_2$/air | CHEMKIN programs using USC Mech II mechanism |
| [18, 23, 24] | $CH_4/O_2/CO_2$ | CHEMKIN programs using GRI-Mech 3.0 mechanism |
| [19] | $CH_4/CO_2$/air | CHEMKIN programs using GRI-Mech 3.0 and C1-C3 reaction mechanisms |
| [21] | $CH_4/CO_2$/air | CHEMKIN programs using Le Cong mechanism |
| [22] | $CH_4/CO_2$/air | Chem1D code using San Diego, GRI-Mech 3.0, USC Mech II, and Konnov mechanisms |
| [7] | $CH_4/CO_2$/air | CANTERA code using GRI-Mech 3.0 mechanism |

Fig. 3 shows experimental and numerical values of laminar burning speed for $CH_4$/air mixtures at standard conditions for varying equivalence ratios. This figure displays that most of the laminar burning speed values for stoichiometric mixtures are approximately $36.5 \pm 1$ cm/s. For increasing equivalence ratio, the laminar burning speed is observed to increase first and then is observed to decrease, after it reaches its maximum at equivalence ratios ($\phi$) of $1.07 \pm 0.01$.

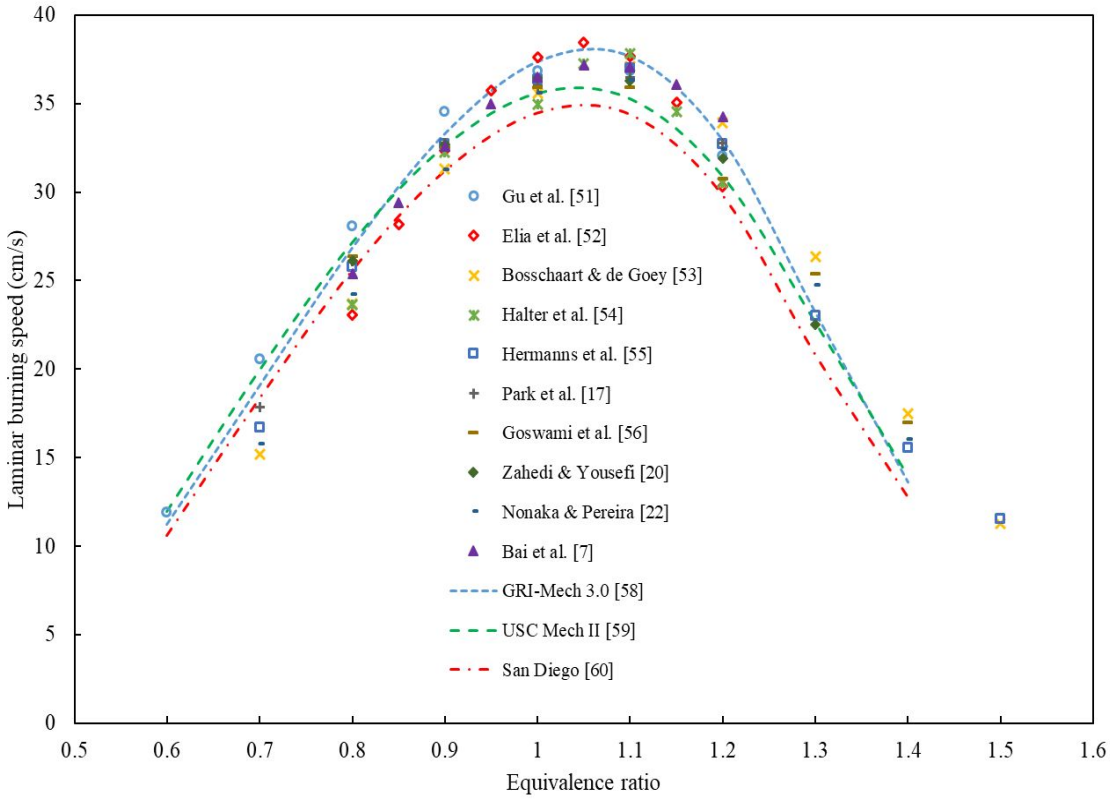


Fig. 3. Laminar burning speed of $CH_4$/air blends for varying equivalence ratios and at standard conditions.

Figs. 4–6 show experimental and numerical values of laminar burning speed for $CH_4/CO_2$/air mixtures at standard conditions for varying equivalence ratios with a different $CO_2$ concentration in each figure. Carbon dioxide concentration in Fig. 3 is 0%, in Fig. 4 is 20%, in Fig. 5 is 40%, in Fig. 6 is 60%.

Fig. 7 compares the laminar burning speed of $CH_4/CO_2$/air blends for different $CO_2$ concentrations versus equivalence ratio in a single plot. In this figure, the experimental data was taken from Bai et al. [7], and numerical results are calculated by GRI-Mech 3.0 [58] mechanism. As shown in Figs. 3–7, laminar burning speed decreases with an increase of $CO_2$ concentration and the maximum laminar burning speeds shift toward stoichiometric mixture as the percentage of $CO_2$ increases in both experimental and numerical results. The influence of $CO_2$ on laminar burning speed is discussed later in this section.

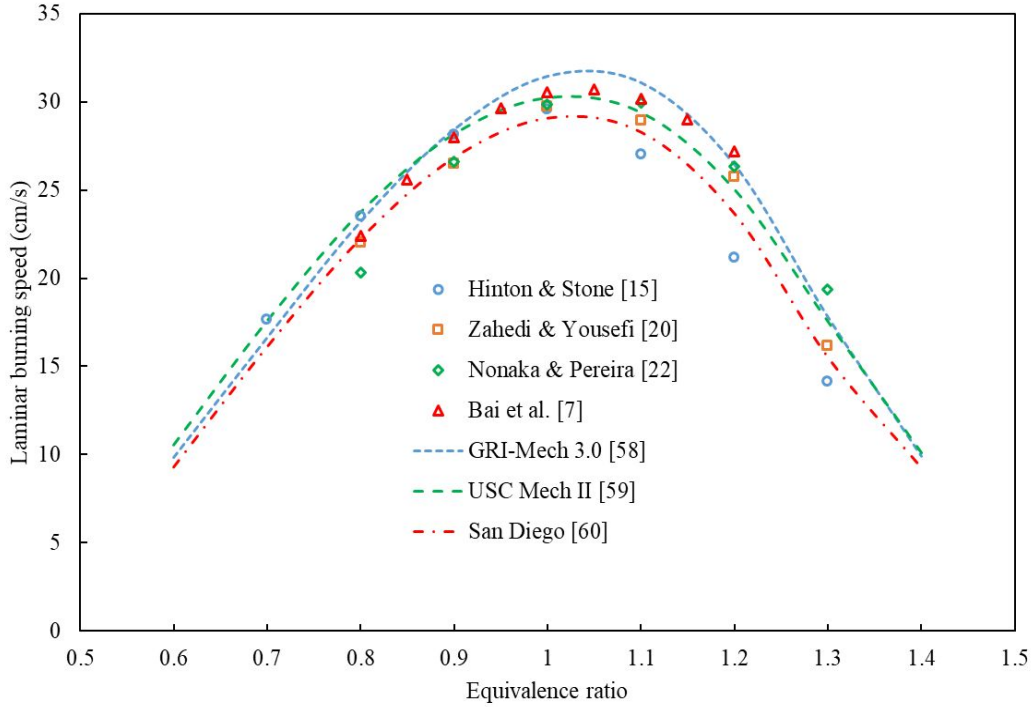


Fig. 4. Laminar burning speed of $CH_4/CO_2$/air blends at varying equivalence ratios, $CO_2$ concentration of 20%, and standard conditions.

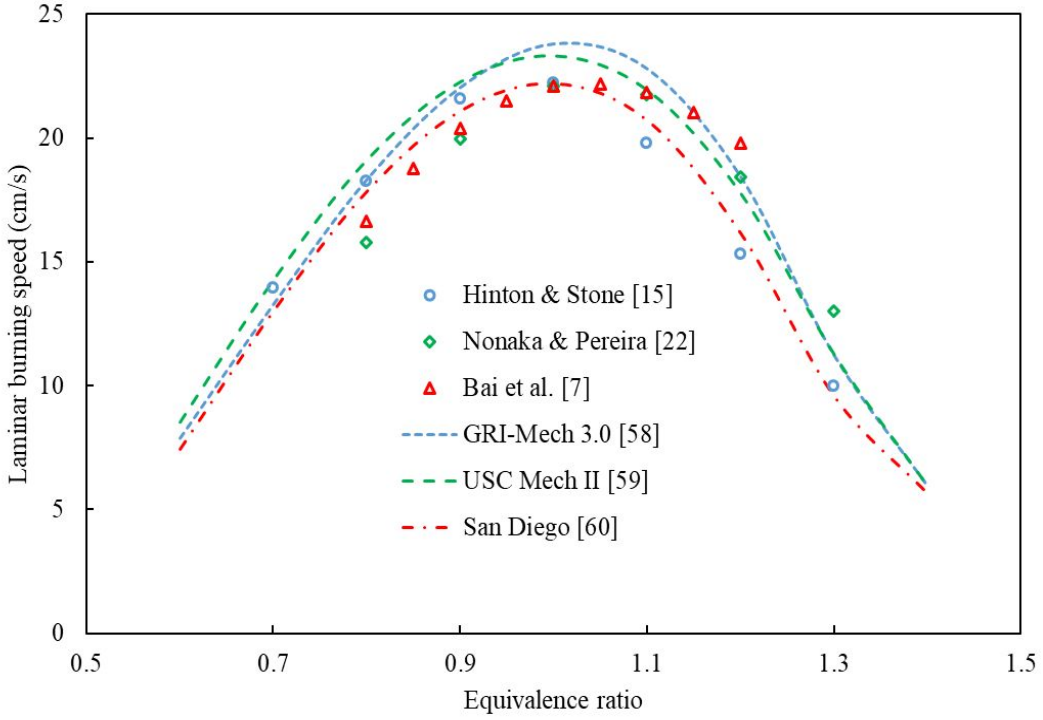


Fig. 5. Laminar burning speed of $CH_4/CO_2$/air blends at varying equivalence ratios, $CO_2$ concentration of 40%, and standard conditions.

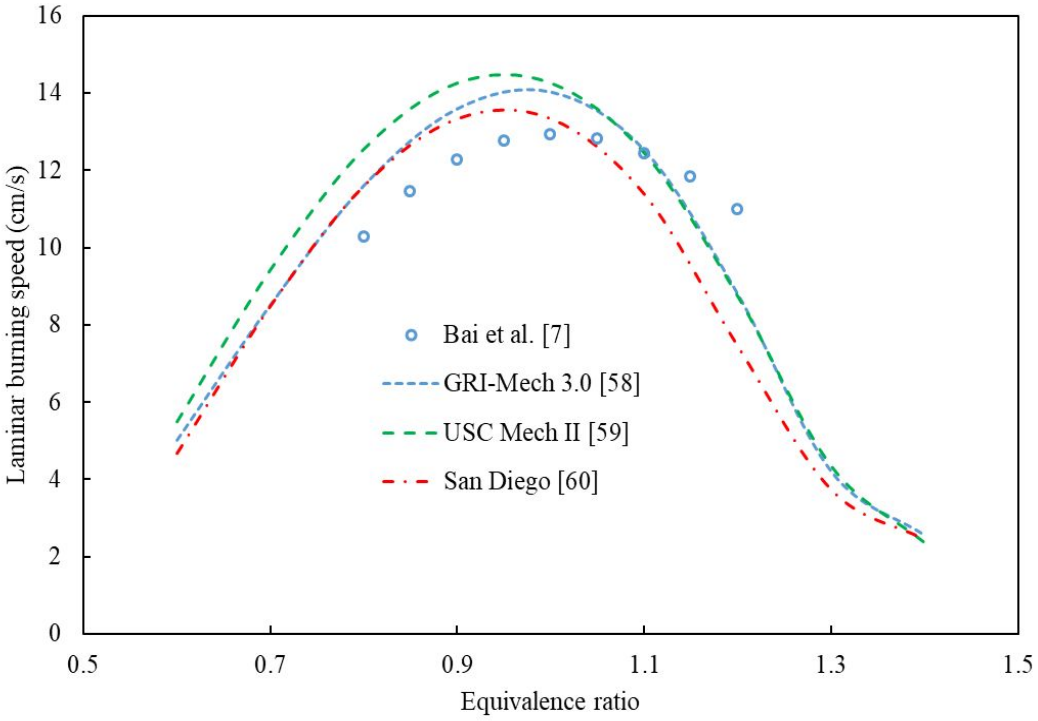


Fig. 6. Laminar burning speed of $CH_4/CO_2$/air blends at varying equivalence ratios, $CO_2$ concentration of 60%, and standard conditions.

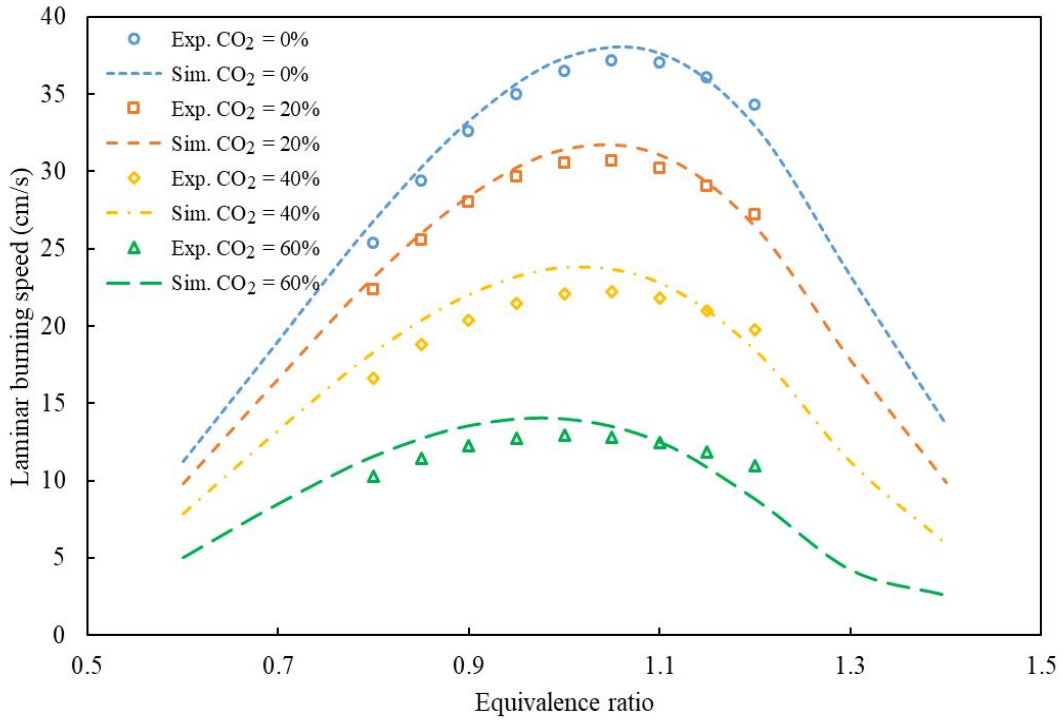


Fig. 7. Laminar burning speed of $CH_4/CO_2$/air blends at varying equivalence ratios and standard conditions for various $CO_2$ mole fractions [7,58].

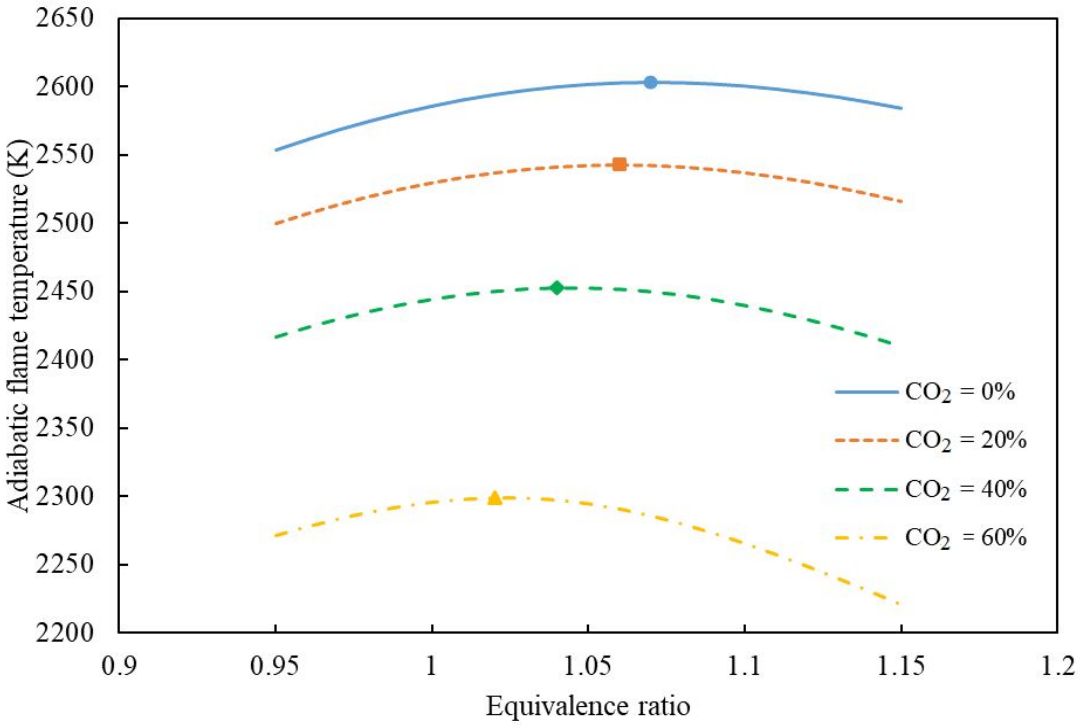


Fig. 8. Equilibrium adiabatic flame temperature of $CH_4/CO_2$/air blends along varying equivalence ratios and standard conditions for various $CO_2$ mole fractions.

Fig. 8 shows equilibrium adiabatic flame temperature of $CH_4/CO_2$/air as calculated by STANJAN [61]. As $CO_2$ concentration increases, the equilibrium adiabatic flame temperature decreases because of the high heat capacity of $CO_2$, which in turn acts as an energy sink. However, equilibrium adiabatic flame temperature is observed to decrease nonlinearly with increasing $CO_2$ concentration. It has a stronger thermal effect for higher $CO_2$ mole fractions in the blends [18]. The direct chemical participation of $CO_2$ also reduces the rate of exothermic reaction $CO + OH = CO_2 + H$, which results in a temperature reduction. Markers on the trends in Fig. 8 indicate the maximum equilibrium adiabatic flame temperature of each case. A shift of equivalence ratio for the maximum equilibrium adiabatic flame temperature from 1.07 to 1.02 can be observed when $CO_2$ concentration changes from 0% to 60%. This shift of maximum flame temperature relates to the shift of maximum laminar burning speed to stoichiometric ratios for $CO_2$ concentrations of 0–60%.

The GRI-Mech 3.0 mechanism was used to perform sensitivity analysis of laminar burning speed for $CH_4/CO_2$/air mixture. Fig. 9 illustrates normalized sensitivity coefficients of laminar burning speed at standard condition and for stoichiometric mixture and different $CO_2$ concentrations. A normalized sensitivity coefficient is defined as $\frac{k\,dS_u}{S_u\,dk}$, where $k$ is the reaction rate constant. The sensitivity factors of laminar burning speed are observed to be affected by increasing $CO_2$ concentrations in $CH_4/CO_2$/air flames. This figure shows the largest positive sensitivity coefficient for the reaction $H + O_2 = O + OH$ and is followed

by $CO + OH = CO_2 + H$. The reverse reaction $CO + OH = CO_2 + H$ is considered as the main pathway where $CO_2$ plays a role in chemical reactions [22]. The direct involvement of $CO_2$ reduces the rate of reaction $CO + OH = CO_2 + H$. Since this is a primary exothermic reaction in the mechanism, a temperature reduction results from the decrease of energy release rate. With the addition of $CO_2$, the H radicals compete among the reaction $H + O_2 = O + OH$ and the reverse reaction $CO + OH = CO_2 + H$. Therefore, the reaction $H + O_2 = O + OH$ is restricted by the existence of $CO_2$, which subsequently inhibits the combustion process [22].

As $CO_2$ concentration increases, $CO_2$ mole fraction in unburned mixture increases at the same equivalence ratio. Due to the nonlinear thermal effect of $CO_2$ and chemical reaction effect of $CO_2$ mentioned above, the leaner mixture (less $CO_2$ content) seems to have a higher equilibrium adiabatic flame temperature. Thus, the higher $CO_2$ mole fraction in an unburned mixture shifts the maximum equilibrium adiabatic flame temperature to leaner equivalence ratios. Which explains the cause of shifting maximum laminar burning speeds toward stoichiometric mixtures.

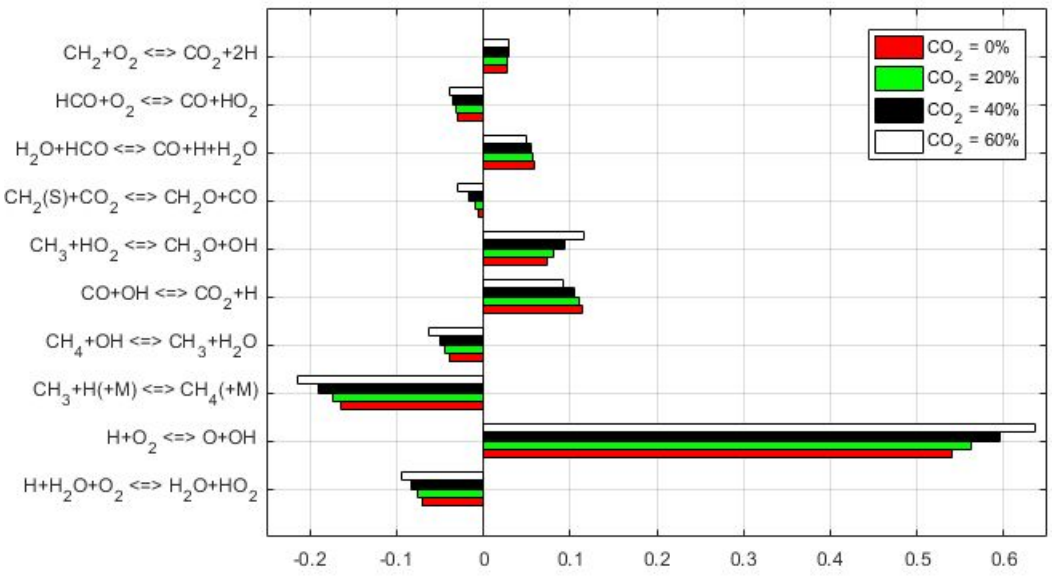


Fig. 9. Normalized sensitivity coefficients of $CH_4/CO_2$/air blends at stoichiometric and standard conditions for various $CO_2$ mole fractions.

### 3.2. Propane/carbon dioxide/air

Different experimental approaches of laminar burning speed measurement in literature [12, 25, 26, 36, 53, 62–69] were mentioned in Section 2. Experimental and numerical values of laminar burning speeds for $C_3H_8/CO_2$/air mixtures are presented in this section. In this paper, numerical results were calculated using the same methodology as $CH_4/CO_2$/air using two chemical kinetic mechanisms: USC Mech II [59] and San Diego [60]. Table 4 lists different numerical methods burning $C_3H_8/CO_2$/air blends.

Table 4. Literature on numerical calculation of laminar burning speed for $C_3H_8/CO_2$/air blends

| Ref. | Mixture | Numerical Method |
|---|---|---|
| [25] | $C_3H_8/CO_2$/air | CHEMKIN programs using C1-C3 reaction and Konnov mechanisms |
| [12] | $C_3H_8/CO_2$/air | CANTERA code using USC Mech II mechanism |

Fig. 10 showcases the experimental and numerical laminar burning speeds of a $C_3H_8$/air mixture at standard condition for varying equivalence ratio. This figure displays that most of the laminar burning speed values for stoichiometric mixtures are approximately $39.5 \pm 1$ cm/s. For increasing equivalence ratio, the laminar burning speed is observed to increase first and then is observed to decrease, after it reaches its maximum at equivalence ratios ($\phi$) of $1.09 \pm 0.01$.

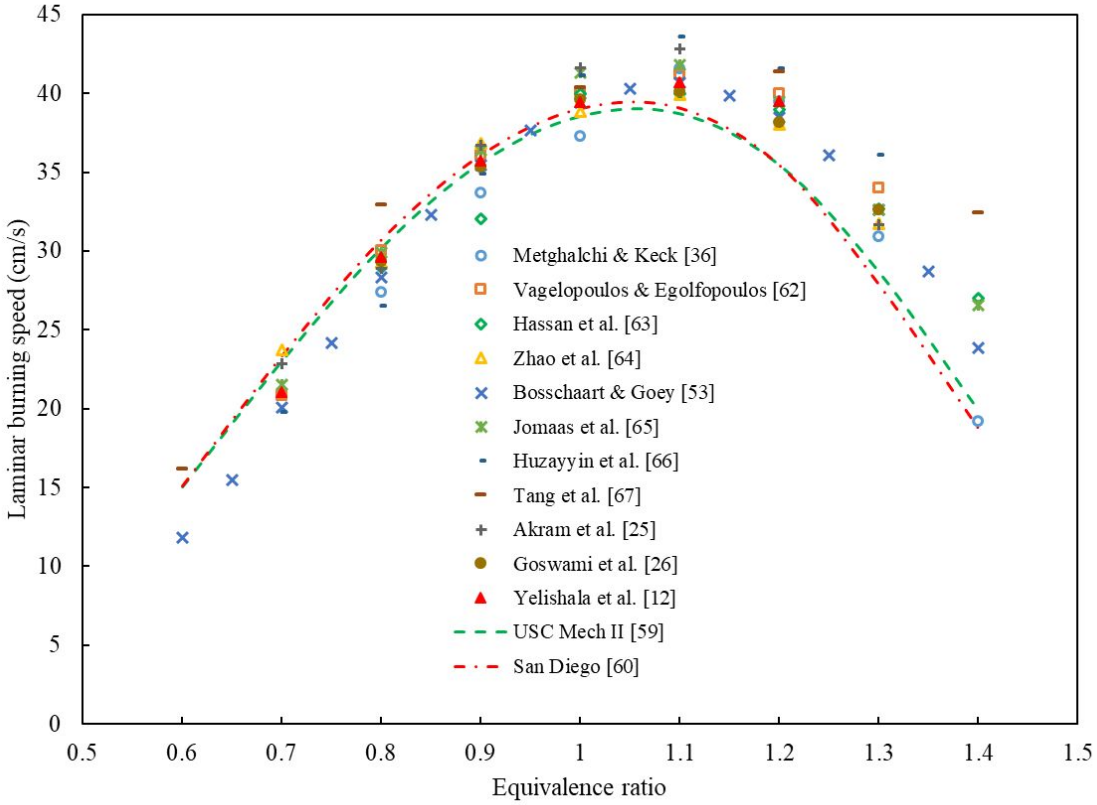


Fig. 10. Laminar burning speed of $C_3H_8$/air blends for varying equivalence ratios and at standard conditions.

Figs. 11–13 show the experimental and numerical values of laminar burning speeds for $C_3H_8/CO_2$/air mixtures versus different equivalence ratios at standard condition. While temperature and pressure have been fixed in these figures, carbon dioxide concentrations have been varied from 0% to 80%. Fig. 14 shows comparison of laminar burning speeds for $C_3H_8/CO_2$/air mixtures versus equivalence ratio for different $CO_2$ concentrations. In

this figure, experimental data was taken from Yelishala et al. [12] and simulation results are calculated using the USC Mech II [59] mechanism. Similar to $CH_4/CO_2$/air mixtures, laminar burning speed decreases with an increase of $CO_2$ concentrations and the maximum laminar burning speed shifts towards leaner mixtures with an increase of $CO_2$ concentrations in both experimental and numerical studies. As shown in Fig. 15, the maximum equilibrium adiabatic flame temperature calculated by STANJAN shifts from $\phi = 1.09$ to $\phi = 1.03$. This phenomenon is due to the high heat capacity of $CO_2$, which in turn acts as an energy sink. However, it is noted that the equilibrium adiabatic flame temperature decreases nonlinearly with the increase of $CO_2$ concentration. It has a stronger thermal effect for a higher $CO_2$ concentration in the mixture [18]. The direct chemical participation of $CO_2$ also reduces the rate of exothermic reaction $CO + OH = CO_2 + H$, which results in a temperature reduction. Markers on the trends in Fig. 15 present the maximum equilibrium adiabatic flame temperature of each case. This shift can be explained in the same way as for the $CH_4/CO_2$/air flame.

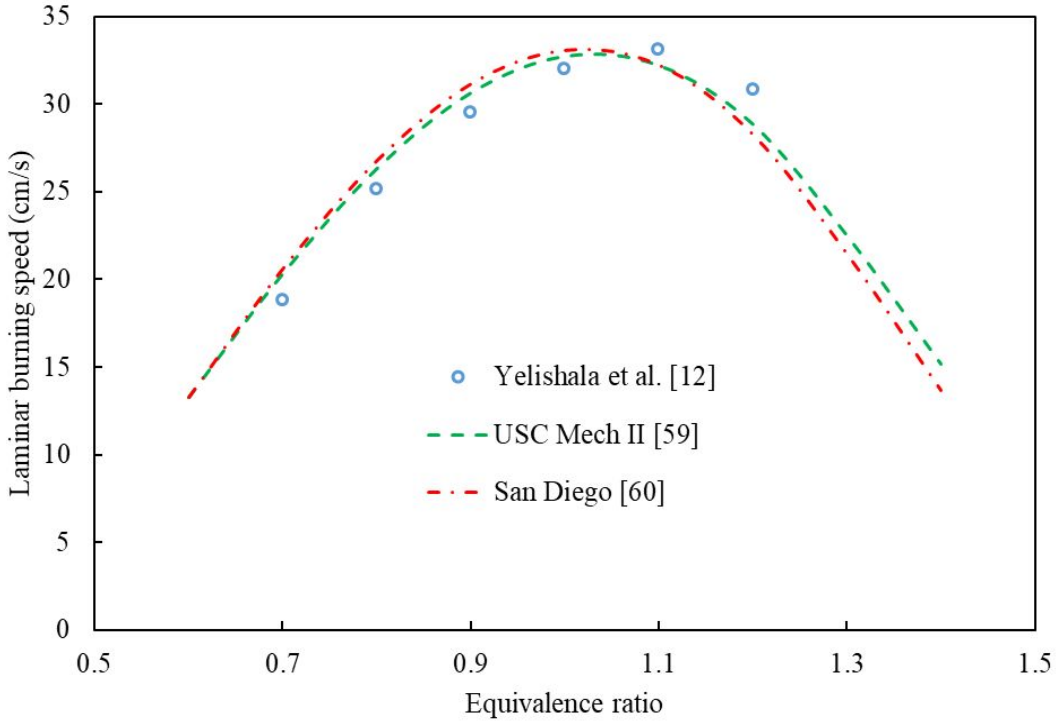


Fig. 11. Laminar burning speed of $C_3H_8/CO_2$/air blends at varying equivalence ratios, $CO_2$ concentration of 20%, and standard conditions.

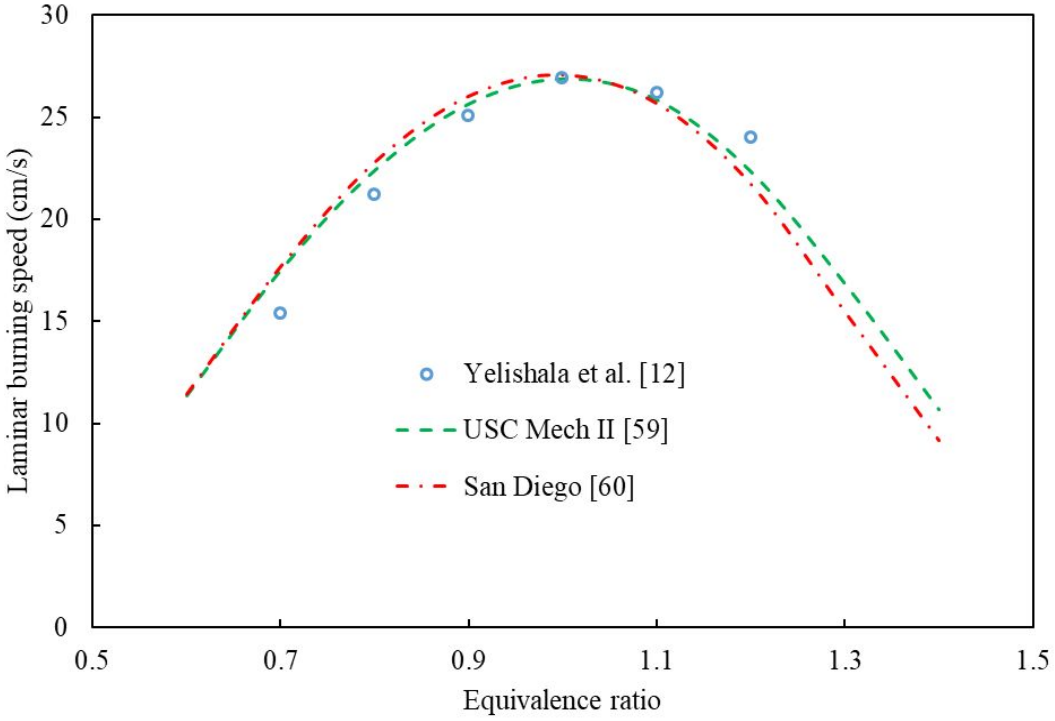


Fig. 12. Laminar burning speed of $C_3H_8/CO_2$/air blends at varying equivalence ratios, $CO_2$ concentration of 60%, and standard conditions.mixture at various equivalence ratios.

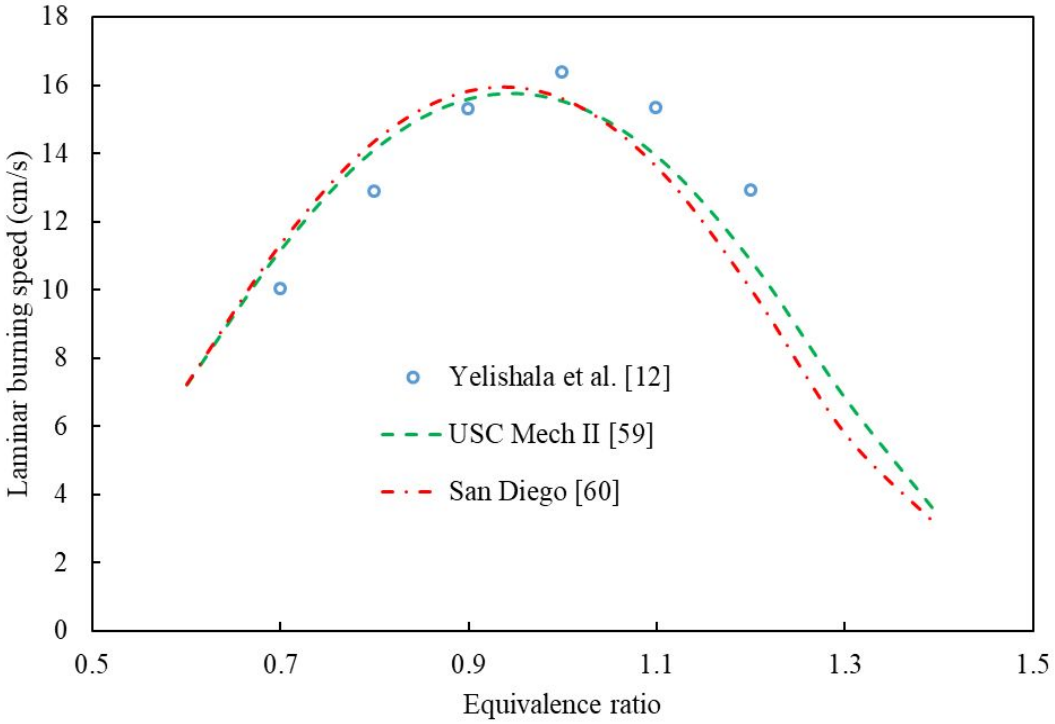


Fig. 13. Laminar burning speed of $C_3H_8/CO_2$/air blends at varying equivalence ratios, $CO_2$ concentration of 80%, and standard conditions.

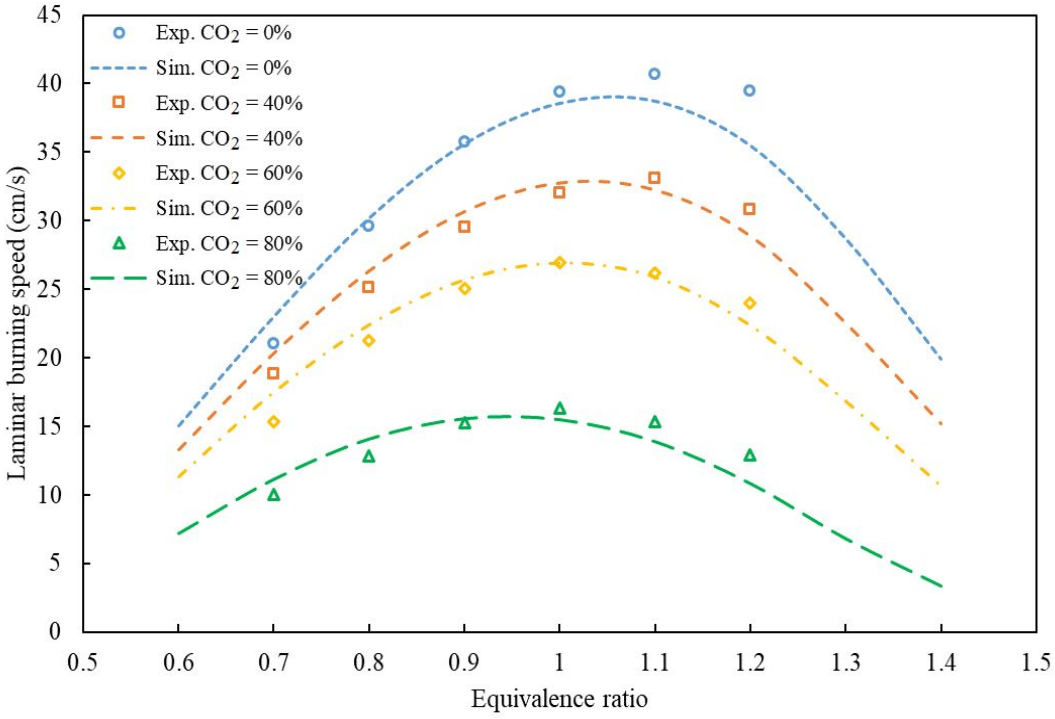


Fig. 14. Laminar burning speed of $C_3H_8/CO_2$/air blends at varying equivalence ratios and standard conditions for various $CO_2$ mole fractions [12,59].

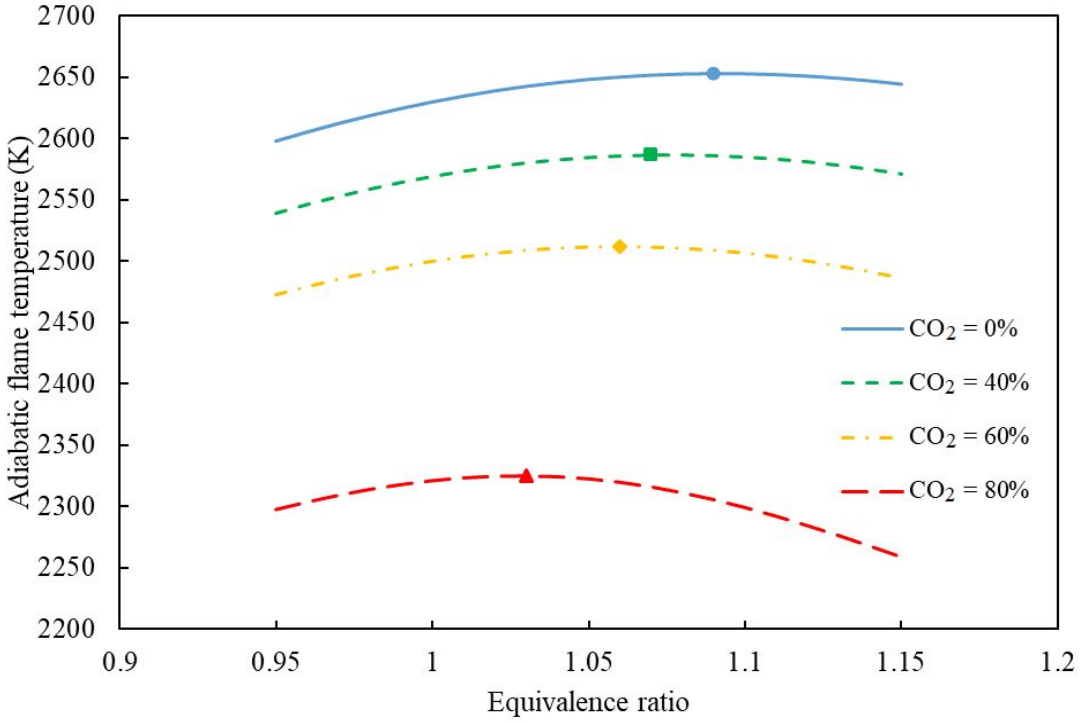


Fig. 15. Equilibrium adiabatic flame temperature of $C_3H_8/CO_2$/air blends along varying equivalence ratios and standard conditions.

A sensitivity analysis of laminar burning speed for a $C_3H_8/CO_2$/air mixture has also been done using the USC Mech II mechanism. Fig. 16 shows the normalized sensitivity coefficients of laminar burning speed for stoichiometric mixture and different $CO_2$ fractions at standard condition. It can be noted that $CO_2$ fraction affect the sensitivity factors of laminar burning speed for $C_3H_8/CO_2$/air flame. This figure shows the largest positive sensitivity coefficient for the reaction $H + O_2 = O + OH$ and is followed by $CO + OH = CO_2 + H$. Similar to the $CH_4/CO_2$/air flame, the direct involvement of $CO_2$ in chemical reaction and the nonlinear thermal effect of $CO_2$ shifts the maximum laminar burning speed of the $C_3H_8/CO_2$/air mixture [70, 71].

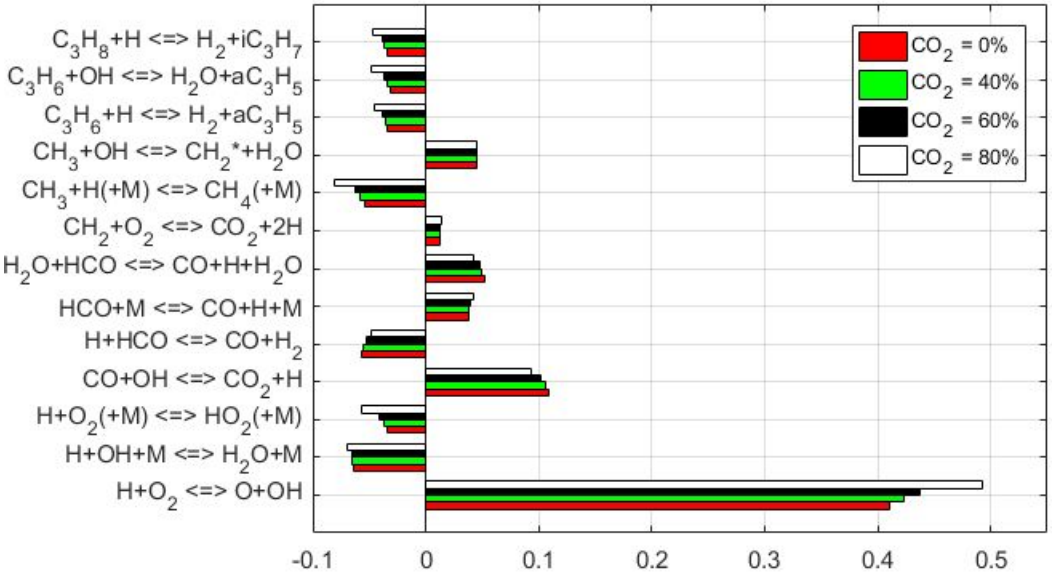


Fig. 16. Normalized sensitivity coefficients of $C_3H_8/CO_2$/air blends at stoichiometric and standard conditions for various $CO_2$ mole fractions.

The combined uncertainty of constant volume method with multi-shell thermodynamic model is calculated as follows [7, 12]

$$E(S_u) = \sqrt{\sum_{i=1}^{n} \left(\frac{\partial f}{\partial x_i}\right)^2 E_i^2(x_i)} \tag{8}$$

where $E(S_u)$ is the uncertainty of $S_u$ related to $x_i$ (temperature, pressure, equivalence ratio, diluent, model) and sensitivity coefficient $\partial f/\partial x_i$. The combined uncertainty of this measurement is predicted to be 3% using Eq. (8).

## 4. Effects of $CO_2$ on flame instability

Three primary instabilities: Rayleigh-Taylor instability, hydrodynamic instability, and thermal-diffusive instability [72–75] are common in combustion study. Rayleigh-Taylor instability was first recognized by Lord Rayleigh [76] and later by Geoffrey Ingram Taylor

[77]. The flame interface is destabilized by the buoyancy effect of lighter burned gas and gravity effect of heavier unburned gas. This instability is neglected in this study due to the relatively high laminar burning speed of methane and propane. Hydrodynamic instability was independently described by Darrieus and Landau [78,79]. This instability is caused by the gas expansion because of the energy released by chemical reactions and is governed by flame thickness and expansion ratio, which always destabilize the flame. Hydrodynamic instability will be enhanced due to the decrease of flame thickness or the increase of expansion ratio. Thermal-diffusive instability is caused by the inequality of thermal and mass diffusion of different species, which is determined by the effective Lewis number [80]. Li and his co-works [81–84] also studied flame instability and other combustion properties of $CH_4$ and $C_3H_8$.

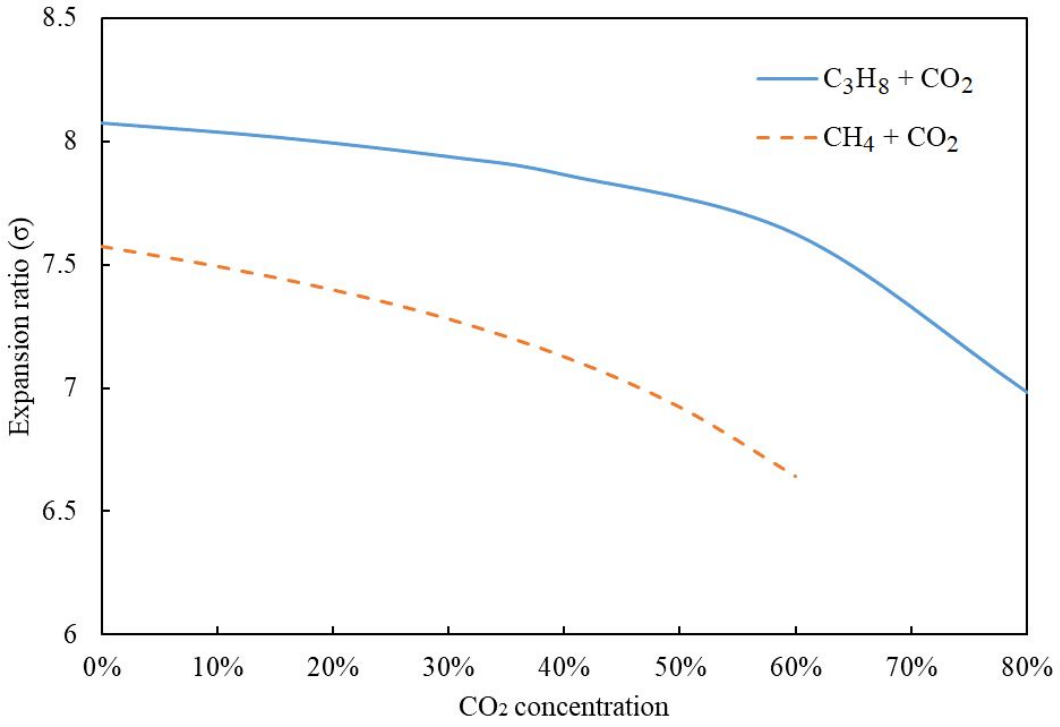


Fig. 17. Expansion ratio of $CH_4/CO_2$/air and $C_3H_8/CO_2$/air at stochiomatic mixture, standard temperature, and pressure of 2 atm.

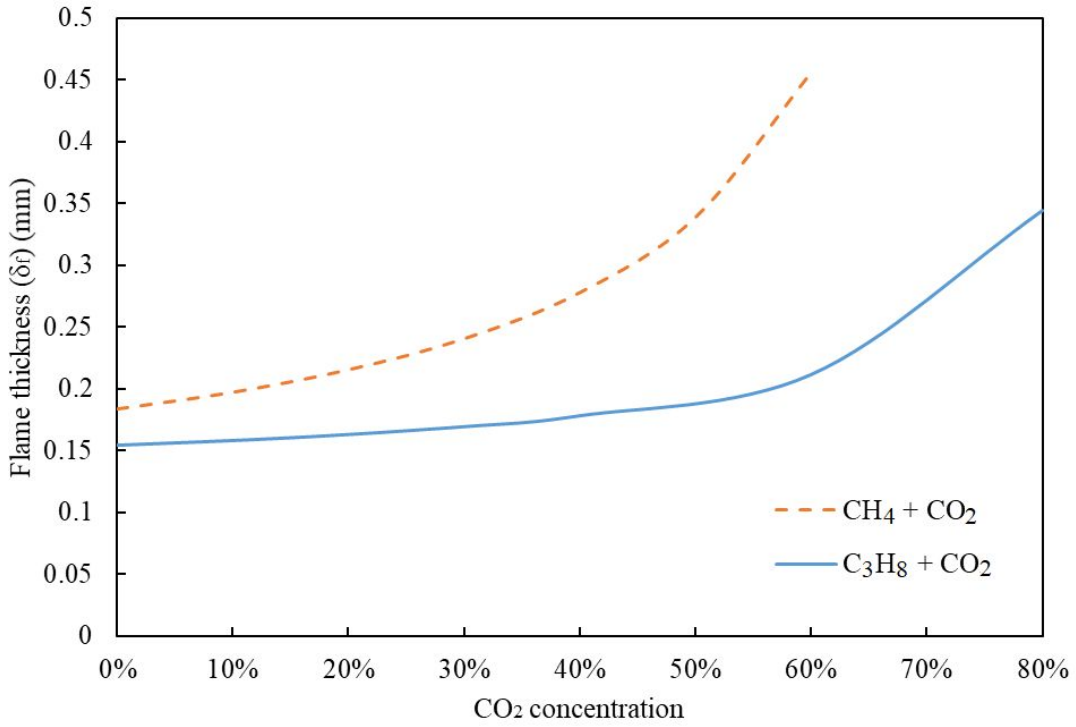


Fig. 18. Flame thickness of $CH_4/CO_2$/air and $C_3H_8/CO_2$/air at stochiomatic mixture, standard temperature, and pressure of 2 atm.

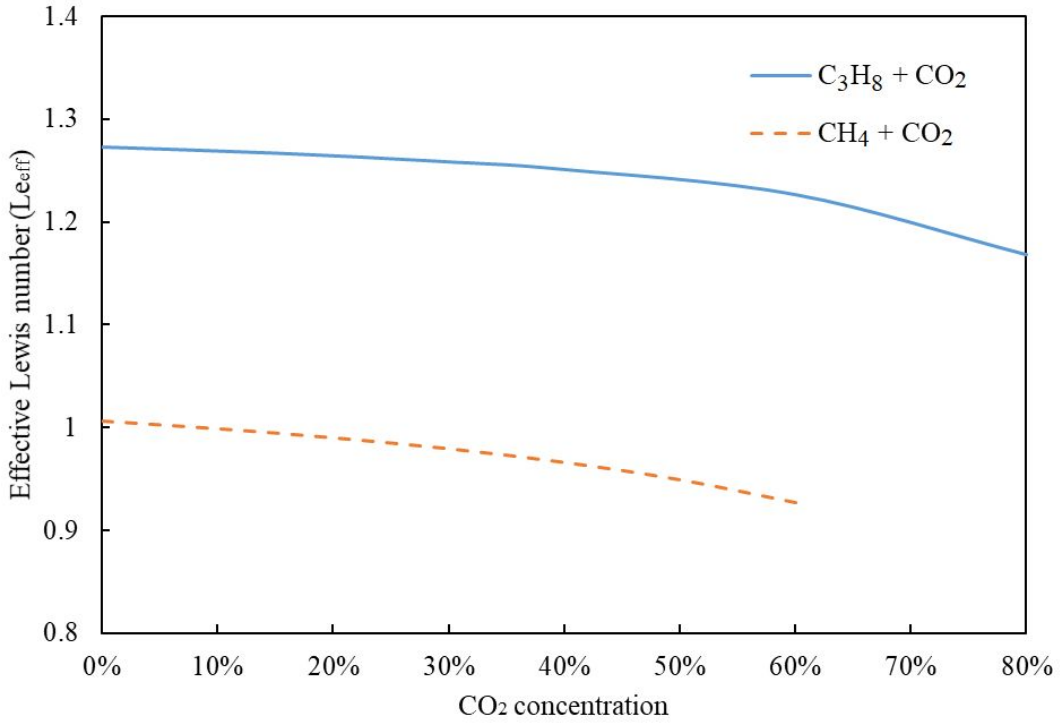


Fig. 19. Effective Lewis number of $CH_4/CO_2$/air and $C_3H_8/CO_2$/air at stochiomatic mixture, standard temperature, and pressure of 2 atm.

Figs. 17–19 show the thermal expansion ratio, flame thickness, and effective Lewis number for $CH_4/CO_2$/air and $C_3H_8/CO_2$/air flames versus $CO_2$ concentration. The thermal expansion ratio is defined by $\sigma = \frac{\rho_u}{\rho_b}$, the flame thickness is defined by $\delta_f = \frac{\alpha}{S_u}$, the Lewis number is defined by $Le = \frac{\alpha}{D}$, where α and $D$ are the thermal and mass diffusivities. The effective Lewis number is defined by

$$Le_{eff} = 1 + \frac{(Le_{Ex} - 1) + (Le_{Def} - 1)A}{1 + A} \quad (8)$$

where $Le_{Ex} = \frac{\alpha_{Ex}}{D_{Ex}}$ is the Lewis number of excessive reactants and $Le_{Def} = \frac{\alpha_{Def}}{D_{Def}}$ is the Lewis number of deficient reactants. $A = 1 + Ze(\frac{1}{\phi} - 1)$, $Ze$ is the flame Zeldovich number calculated as follows

$$Ze = \frac{E_a(T_b - T_u)}{\overline{R}T_b^2} \quad (9)$$

where $E_a = -2\overline{R}\frac{\partial \ln (S_u \rho_u)}{\partial \ln (1/T_b)}$ is the global activation energy and $\overline{R}$ is the universal gas constant [46]. With an increase of $CO_2$ concentration in both $CH_4$ and $C_3H_8$ flames, the flame thickness increases while the expansion ratio decreases, which suppresses hydrodynamic instability. However, the effective Lewis number decreases as $CO_2$ concentration increases in both $CH_4$ and $C_3H_8$ flames, which promotes thermal-diffusive instability.

As shown in Fig. 20, flames become more stable as the concentration of $CO_2$ increases for various equivalence ratios. It shows that $CO_2$ suppresses flame instability as a consequence of the combination of thermal-diffusive and hydrodynamic effects.

| | 0% | 20% | 40% | 60% |
|---|---|---|---|---|

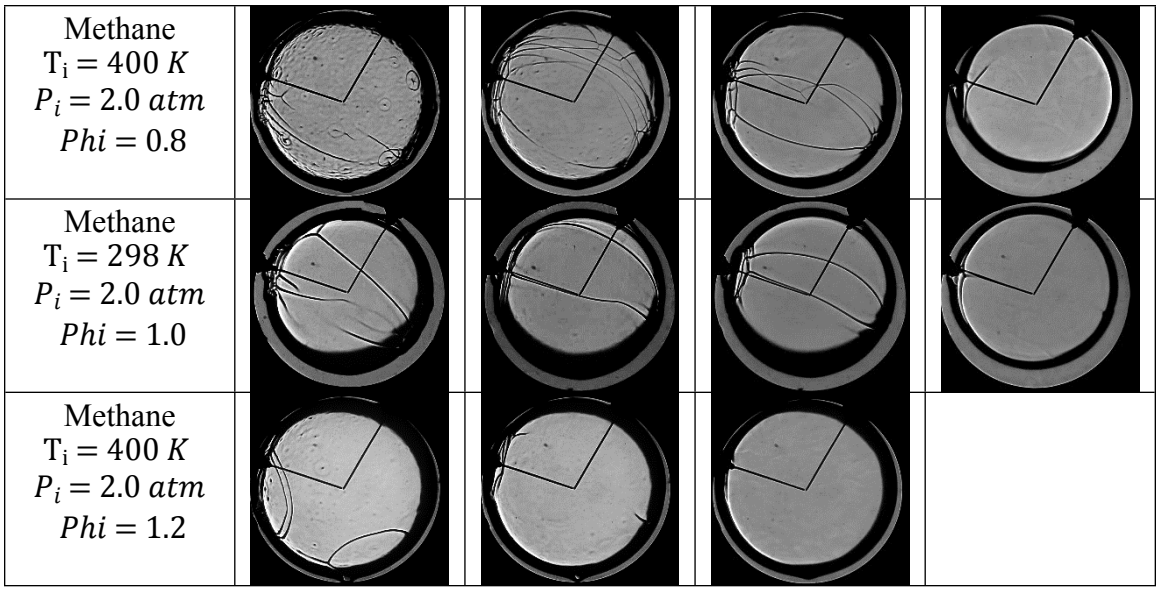


Fig. 20. Snapshots of $CH_4/CO_2$/air blends at two different initial temperatures and initial pressure of 2 atm [7].

## 5. Conclusions

The available literature for laminar burning speed and flame instability of $CH_4/CO_2$/air and $C_3H_8/CO_2$/air blends has been reviewed. The results are summarized as follows:

(1) Laminar burning speeds and equilibrium adiabatic flame temperatures of $CH_4/CO_2$/air and $C_3H_8/CO_2$/air combustion decrease with the addition of $CO_2$. Laminar burning speeds of stoichiometric $CH_4/CO_2$/air and $C_3H_8/CO_2$/air were measured to be around 36.5 cm/s and 39.5 cm/s, respectively. Addition of $CO_2$ reduced such speeds significantly, for instance 60% $CO_2$ reduced these speeds to around 12.5 cm/s and 26.5 cm/s, respectively.

(2) Carbon dioxide contributes in the chemical reaction mainly via the reverse reaction of $CO + OH = CO_2 + H$ and slows down the flame by competing for the H radical with reaction $H + O_2 = O + OH$.

(3) As $CO_2$ concentration increases, the maximum laminar burning speed shifts toward stoichiometric mixture because of the thermal and chemical effects.

(4) As $CO_2$ concentration increases, thermal-diffusive instability is promoted while hydrodynamic instability is inhibited in both $CH_4/CO_2$/air and $C_3H_8/CO_2$/air flames. Carbon dioxide suppresses flame instability as a consequence of the combination of thermal-diffusive and hydrodynamic effects.

**Acknowledgments**

This research is funded by the American Chemical Society (ACS), Petroleum Research Fund (RPF#59069-ND9; Funder ID: 10.13039/100006770).

**References**

[1] Noyola, A.; Morgan-Sagastume, J. M.; Lopez-Hernandez, J. E. Treatment of biogas produced in anaerobic reactors for domestic wastewater: odor control and energy/resource recovery. *Rev Environ Sci Bio technol*. 2006, 5(1), 93–114.

[2] Pizzuti, L.; Martins, C. A.; Lacava, P. T. Laminar burning velocity and flammability limits in biogas: A literature review. *Renewable and Sustainable Energy Reviews* 2016, 62, 856–865.

[3] Huang, J.; Crookes, R. J. Assessment of simulated biogas as a fuel for the spark ignition engine. *Fuel* 1998, 77, 1793–1801.

[4] Crookes, R. J. Comparative bio-fuel performance in internal combustion engines. *Biomass Bioenergy* 2006, 30(5), 461–468.

[5] Shrestha, S. O.; Narayanan, G. Landfill gas with hydrogen addition–a fuel for SI engines. *Fuel* 2008, 87, 3616–3626.

[6] Porpatham, E.; Ramesh, A.; Nagalingam, B. Investigation on the effect of concentration of methane in biogas when used as a fuel or a spark ignition engine. *Fuel* 2008, 87, 1651–1659.

[7] Bai, Z.; Wang, Z.; Yu, G.; Yang, Y.; Metghalchi, H. Experimental Study of Laminar Burning Speed for Premixed Biomass/Air Flame. *J. Energy Resour. Technol.* 2018, 141(2), 022206.

[8] Ashok, B.; Ashok, D. S.; Kumar, R. C. LPG Diesel Dual Fuel Engine–A Critical Review. *Alexandra Eng. J.* 2015, 54(2), 105–126.

[9] Pourkhesalian, A. M.; Shamekhi, A. H.; Salimi, F. Alternative Fuel and Gasoline in an SI Engine: A Comparative Study of Performance and Emissions Characteristics. *Fuel* 2010, 89(5), 1056–1063.

[10] Mardi, M.; Khalilarya, S.; Nemari, A. A Numerical Investigation on the Influence of EGR in a Supercharged SI Engine Fueled with Gasoline and Alternative Fuels. *Energy Convers. Manage.* 2014, 83, 260–269.

[11] Nair, A.; Kishore, V. R.; Kumar, S. Effect of $CO_2/N_2$ dilution on laminar burning velocity of liquid petroleum gas-air mixtures at elevated temperatures. *Energy* 2016, 100, 145–153.

[12] Yelishala, S. C.; Wang, Z.; Metghalchi, H.; Levendis, Y.A.; Kannaiyan, K.; Sadr, R. Effect of Carbon Dioxide on the Laminar Burning Speed of Propane–Air Mixtures. *J. Energy Resour. Technol.* 2019, 141(2), 082205.

[13] ANSI/ASHRAE. Safety Standard for Refrigeration Systems American Society of Heating, Refrigerating and Air-Conditioning Engineers. Atlanta, GA, 2013, Standard No. 15-2013.

[14] Stone, R.; Clarke, A. Correlations for the Laminar Burning Velocity of Methane/Diluent/Air Mixtures Obtained in Free-Fall Experiments. *Combustion and flame* 1998, 114, 546–555.

[15] Hinton, N.; Stone, R.; Laminar burning velocity measurements of methane and carbon dioxide mixtures (biogas) over wide ranging temperatures and pressures. *Fuel* 2014, 116, 743–750.

[16] Kishore, V. R.; Duhan, N.; Ravi, M. R.; Ray A. Measurement of adiabatic burning velocity in natural gas-like mixtures. *Experimental Thermal and Fluid Science* 2008, 33, 10–16.

[17] Park, O.; Veloo, P. S.; Liu, N.; Egolfopoulos, F. N. Combustion characteristics of alternative gaseous fuels. *Proceedings of the Combustion Institute* 2011, 33, 887–894.

[18] Xie, Y.; Wang, J.; Zhang, M.; Gong, J.; Jin, W.; Huang, Z. Experimental and Numerical Study on Laminar Flame Characteristics of Methane Oxy-fuel Mixtures Highly Diluted with $CO_2$. *Energy Fuels* 2013, 27, 6231−6237.

[19] Cardona, C. A.; Amell, A. A. Laminar burning velocity and interchangeability analysis of biogas/$C_3H_8$/$H_2$ with normal and oxygen-enriched air. *International Journal of Hydrogen Energy* 2013, 38, 7994−8001.

[20] Zahedi, P.; Yousefi, K. Effects of pressure and carbon dioxide, hydrogen and nitrogen concentration on laminar burning velocities and NO formation of methane–air mixtures. *Journal of Mechanical Science and Technology* 2014, 28(1), 377–386.

[21] Chan, Y.; Zhu, M.; Zhang, Z.; Liu, P.; Zhang, D. The Effect of $CO_2$ Dilution on the Laminar Burning Velocity of Premixed Methane/Air Flames. *Energy Procedia* 2015, 75, 3048–3053.

[22] Nonaka, H. O. B.; Pereira, F. M. Experimental and numerical study of $CO_2$ content effects on the laminar burning velocity of biogas. Fuel 2016, 182, 382–390.

[23] Hu, X.; Yu, Q.; Liu, J.; Sun, N. Investigation of laminar flame speeds of $CH_4$/$O_2$/$CO_2$ mixtures at ordinary pressure and kinetic simulation. *Energy* 2014, 70, 626–634.

[24] Hu, X.; Yu, Q. Effect of the elevated initial temperature on the laminar flame speeds of oxy-methane mixtures. *Energy* 2018, 147, 876–883.

[25] Akram, M.; Kishore, V. R.; Kumar, S. Laminar Burning Velocity of Propane/$CO_2$/$N_2$−Air Mixtures at Elevated Temperatures. *Energy Fuels* 2012, 26, 5509–5518.

[26] Goswami, M.; Bastiaans, R. J. M.; de Goey, L. P. H.; Konnov, A. A. Experimental and modelling study of the effect of elevated pressure on ethane and propane flames. *Fuel* 2016, 166, 410–418.

[27] Fedyaeva, O. N.; Artamonov, D. O.; Vostrikov, A. A. Effect of $H_2O$ and $CO_2$ on propane, propene, and isopropanol oxidation at elevated pressures. *Combustion and Flame* 2019, 199, 230–240.

[28] Egolfopoulos, F. N.; Hansen, N.; Ju, Y.; Kohse-Höinghaus, K.; Law, C. K.; Qi, F. Advances and challenges in laminar flame experiments and implications for combustion chemistry. *Progress in Energy and Combustion Science* 2014, 43, 36–67.

[29] Botha, J. P.; Spalding, D. B. The laminar flame speed of propane/air mixtures with heat extraction from the flame. *Proceedings of Royal Society of London A* 1954, 225, 71–96.

[30] van Maaren, A.; Thung, D. S.; de Goey, L. P. H. Measurement of flame temperature and adiabatic burning velocity of methane/air mixtures. *Combustion Science and Technology* 1994, 96, 327–344.

[31] Wu, C. K.; Law, C. K. On the determination of laminar flame speeds from stretched flames. *Proc Combust Inst.* 1985, 20, 1941–1949.

[32] Yu, G.; Wu, C. K.; Law, C. K. Laminar flame speeds of hydrocarbon air mixtures with hydrogen addition. *Combustion and Flame* 1986, 63(3), 339–347.

[33] Law, C. K.; Zhu, D. L.; Yu, G. Propagation and extinction of stretched premixed flames. *Symp (Int) Combust* 1988, 21, 1419–1426.

[34] Strauss, W. A.; Edse, R. Burning velocity measurements by the constant pressure bomb method. *Symposium (International) Combustion* 1958, 7, 377–385.

[35] Lewis, B.; von Elbe, G. Combustion, Flames and Explosions of Gases, London, UK, Academic Press Inc., 1961.

[36] Metghalchi, M.; Keck, J. C. Laminar burning velocity of propane-air mixtures at high temperature and pressure. *Combust Flame* 1980, 38, 143–154.

[37] Metghalchi, M.; Keck, J. C. Burning velocities of mixtures of air with methanol, isooctane, and indolene at high pressure and temperature. *Combust Flame* 1982, 48, 191–210.

[38] Parsinejad, F.; Arcari, C.; Metghalchi, H. Flame structure and burning speed of JP-10 air mixtures. *Combust Sci Technol* 2006, 178, 975–1000.

[39] Rahim, F.; Eisazadeh-Far, K.; Parsinejad, F.; Andrews, R. J.; Metghalchi, H. A thermodynamic model to calculate burning speed of methane-air-diluent mixtures. *Int J Thermodyn* 2008, 11, 151–161.

[40] Eisazadeh-Far, K.; Moghaddas, A.; Rahim, F.; Metghalchi, H. Burning speed and entropy production calculation of a transient expanding spherical laminar flame using a thermodynamic model. *Entropy* 2010, 12(12), 2485–2496.

[41] Eisazadeh-Far, K.; Parsinejad, F.; Metghalchi, H.; Keck, J. C. On flame kernel formation and propagation in premixed gases. *Combust Flame* 2010, 157(12), 2211–2221.

[42] Eisazadeh-Far, K.; Parsinejad, F.; Metghalchi, H. Flame structure and laminar burning speeds of JP-8/air premixed mixtures at high temperatures and pressures. *Fuel* 2010, 89(5), 1041–1049.

[43] Eisazadeh-Far, K.; Moghaddas, A.; Metghalchi, H.; Keck, J. C. The effect of diluent on flame structure and laminar burning speeds of JP-8/oxidizer/diluent premixed flames. *Fuel* 2011, 90(4), 1476–1486.

[44] Moghaddas, A.; Eisazadeh-Far, K.; Metghalchi, H. Laminar burning speed measurement of premixed n-decane/air mixtures using spherically expanding flames at high temperatures and pressures. *Combust Flame* 2012, 159(4), 1437–1443.

[45] Rokni, E.; Moghaddas, A.; Askari, O.; Metghalchi, H. Measurement of laminar burning speeds and investigation of flame stability of acetylence ($C_2H_2$)/air mixtures. *J Energy Resourc Technol* 2015, 137(1), 012204.

[46] Askari, O.; Moghaddas, A.; Alholm, A.; Vein, K.; Alhazmi, B.; Metghalchi, H. Laminar burning speed measurement and flame instability study of $H_2$/CO/air mixtures at high temperatures and pressures using a novel multi shell model. *Combust Flame* 2016, 168, 20–31.

[47] Askari, O.; Vien, K.; Wang, Z.; Sirio, M.; Metghalchi, H. Exhaust gas recirculation effects on flame structure and laminar burning speeds of $H_2$/CO/air flames at high pressures and temperatures. *Applied Energy* 2016, 179, 451–462.

[48] Askari, O.; Wang, Z.; Vien, K.; Sirio, M.; Metghalchi, H. On the flame stability and laminar burning speeds of syngas/$O_2$/He premixed flame. *Fuel* 2017, 190, 90–103.

[49] Wang, Z.; Alswat, M.; Yu, G.; Allehaibi, M. O.; Metghalchi, H. Flame structure and laminar burning speed of gas to liquid fuel air mixtures at moderate pressures and high temperatures. *Fuel* 2017, 209, 529–537.

[50] Wang, Z.; Bai, Z.; Yelishala, S. C.; Yu, G.; Metghalchi, H. Effects of diluent on laminar burning speed and flame structure of gas to liquid fuel air mixtures at high temperatures and moderate pressures. *Fuel* 2018, 231, 204–214.

[51] Gu, X. J.; Haq, M. Z.; Lawes, M.; Woolley, R. Laminar Burning Velocity and Markstein Lengths of Methane–Air Mixtures. *Combust Flame* 2000, 121, 41–58.

[52] Elia, M.; Ulinski, M.; Metghalchi, M. Lamianr burning velocity of methane-air-diluent mixtures. *Journal of Engineering for Gas Turbines and Power* 2001, 123(1), 190–196.

[53] Bosschaart, K. J.; de Goey, L. P. H. The laminar burning velocity of flames propagating in mixtures of hydrocarbons and air measured with the heat flux method. *Combustion and Flame* 2004, 136, 261–269.

[54] Halter, F.; Chauveau, C.; Djeballi-Chaumeix, N.; Gokalp, I. Characterization of the effects of pressure and hydrogen concentration on laminar burning velocities of methane–hydrogen–air mixtures. *Proc. Combust. Inst.* 2005, 30, 201–208.

[55] Hermanns, R. T. E.; Konnov, A. A.; Bastiaans, R. J. M.; de Goey, L. P. H.; Lucka, K.; Köhne, H. Effects of temperature and composition on the laminar burning velocity of $CH_4$ + $H_2$ + $O_2$ + $N_2$ flames. *Fuel* 2010, 89, 114–21.

[56] Goswami, M.; Derks, S. C. R.; Coumans, K.; Slikker, W. J.; de Andrade Oliveira, M. H.; Bastiaans, R. J. M; Luijten, C. C. M; de Goey, L. P. H.; Konnov, A. A. The effect of elevated pressures on the laminar burning velocity of methane + air mixtures. *Combustion and Flame* 2013, 160, 1627–1635

[57] Goodwin, D.; Moffat, H.; Speth, R. Cantera: an object-oriented software toolkit for chemical kinetics, thermodynamics, and transport processes. 2015 http://www.cantera.org.

[58] Smith, G. P.; Golden, D. M.; Frenklach, M.; Moriarty, N. W.; Goldenberg, B. E. M.; Bowman, C. T.; Hanson, R. K.; Song, S.; Gardiner, W. C.; Lissianski, V. V.; Qin, Z. W. GRI-Mech 3.0; 1999. http://www.me.berkeley.edu/gri_mech/.

[59] Wang, H.; You, X.; Joshi, A. V.; Davis, S. G.; Laskin, A.; Egolfopoulos, F. N.; Law, C. K. High-Temperature Combustion Reaction Model of $H_2$/CO/C1–C4 Compounds. USC Mech Version II; 2007. http://ignis.usc.edu/USC_Mech_II.htm.

[60] Petrova, M. V.; Williams, F. A. A small detailed chemical kinetic mechanism for hydrocarbon combustion. *Combust Flame* 2006, 144, 526–44.

[61] Reynolds, W. C. The Element Potential for Chemical Equilibrium Analysis: Implementation in the Interactive Program STANJAN, Technical Report A-3391, Stanford University, Stanford, CA, 1986.

[62] Vagelopoulos, C. M.; Egolfopoulos, F. N. Direct experimental determination of laminar flame speeds. *Symp (Int) Combust* 1998, 27(1), 513–519.

[63] Hassan, M. I.; Aung, K. T.; Kwon, O. C.; Faeth, G. M. Properties of laminar premixed hydrocarbon/air flames at various pressures. *J Propul Power* 1998, 14, 479–488.

[64] Zhao, Z.; Kazakov, A.; Li, J.; Drier, F. L. The initial temperature and $N_2$ dilution effect on the laminar flame speed of propane/air. *Combust Sci Technol* 2004, 176(10), 1705–1723.

[65] Jomaas, G.; Zheng, X. L.; Zhu, D. L.; Law, C. K. Experimental determination of counterflow ignition temperatures and laminar flame speeds of $C_2$–$C_3$ hydrocarbons at atmospheric and elevated pressures. *Proceedings of the Combustion Institute* 2005, 30, 193–200.

[66] Huzayyin, A. S.; Moneib, H. A.; Shehatta, M. S.; Attia, A. M. A. Laminar burning velocity and explosion index of LPG–air and propane–air mixtures. *Fuel* 2008, 87, 39–57.

[67] Tang, C.; Zheng, J.; Huang, Z.; Wang, J. Study on nitrogen diluted propane–air premixed flames at elevated pressures and temperatures. *Energy Convers Manage* 2010, 51, 288–295.

[68] Yu, G.; Metghalchi, H.; Askari, O.; Wang, Z. Combustion Simulation of Propane/Oxygen (With Nitrogen/Argon) Mixtures Using Rate-Controlled Constrained-Equilibrium. *J. Energy Resour. Technol.* 2019, 141(2), 022204.

[69] Kim, K.; Askari, O. Understanding the Effect of Capacitive Discharge Ignition on Plasma Formation and Flame Propagation of Air–Propane Mixture. *J. Energy Resour. Technol.* 2019, 141(8), 082201.

[70] Yan, C.; Kocevska, S.; Krasnoperov, L. N. Kinetics of the Reaction of $CH_3O_2$ Radicals with OH Studied over the 292–526 K Temperature Range. *The Journal of Physical Chemistry A* 2016, 120(31), 6111–6121.

[71] Sangwan, M.; Yan, C.; Chesnokov, E. N.; Krasnoperov, L. N. Reaction $CH_3 + CH_3 \rightarrow C_2H_6$ Studied over the 292–714 K Temperature and 1–100 bar Pressure Ranges. *The Journal of Physical Chemistry A* 2015, 119(28), 7847–7857.

[72] Zare, S.; Roy, S.; El Maadi, A.; Askari, O. An investigation on laminar burning speed and flame structure of anisole-air mixture. *Fuel* 2019, 244, 120–131.

[73] Roy, S.; Zare, S.; Askari, O. Understanding the Effect of Oxygenated Additives on Combustion Characteristics of Gasoline. *J. Energy Resour. Technol.* 2019, 141(2), 022205.

[74] Law, C. K. Combustion physics. Cambridge university press: Cambridge, UK 2010.

[75] Wang, Z.; Bai, Z.; Yu, G.; Yelishala, S. C.; Metghalchi, H. The Critical Pressure at the Onset of Flame Instability of Syngas/Air/Diluent Outwardly Expanding Flame at Different Initial Temperatures and Pressures. *J. Energy Resour. Technol.* 2019, 141(8), 082207.

[76] Rayleigh, L. Investigation of the character of the equilibrium of an incompressible heavy fluid of variable density. Scientific Papers by Lord Rayleigh, Dover, 1964.

[77] Taylor, G. The instability of liquid surfaces when accelerated in a direction perpendicular to their planes. I. *Proceedings of the Royal Society, A, vol. CCI*, 1950, 192–196.

[78] Darrieus, G. Propagation d'un front de flame, unpublished work presented at Paris. In: La Technique Moderne and le Congres de Mechanique Appliquee; 1938.

[79] Landau, L. D. On the theory of slow combustion. Acta Physicochimica. URSS 1944, 19, 77–88.

[80] Sivashinsky, G. I. Instabilities, pattern-formation, and turbulence in flame. *Annu. Rev. Fluid Mech.* 1983, 15, 179–199.

[81] Yuan, Y.; Li, G.; Sun, Z.; Li, H.; Zhou, Z. Numerical study of the effects of the channel and nozzle wall on the transition behavior of a methane tribrachial flame in a confined flow. *Fuel* 2019, 160, 366–374.

[82] Yuan, Y.; Li, G.; Sun, Z.; Li, H.; Zhou, Z. Experimental study on the dynamical features of a partially premixed methane jet flame in coflow. *Energy* 2016, 111, 593–598.

[83] Li, H.; Li, G.; Sun, Z.; Zhou, Z.; Li, Y.; Yuan, Y. Fundamental Combustion Characteristics of Lean and Stoichiometric Hydrogen Laminar Premixed Flames Diluted with Nitrogen or Carbon Dioxide. *Journal of Engineering for Gas Turbines and Power* 2016, 138, 111501.

[84] Jiang, Y.; Li, G.; Li, H.; Li, L.; Zhang, G. Effect of flame inherent instabilities on the flame geometric structure characteristics based on wavelet transform. *International Journal of Hydrogen Energy* 2018, 43, 9022–9035.

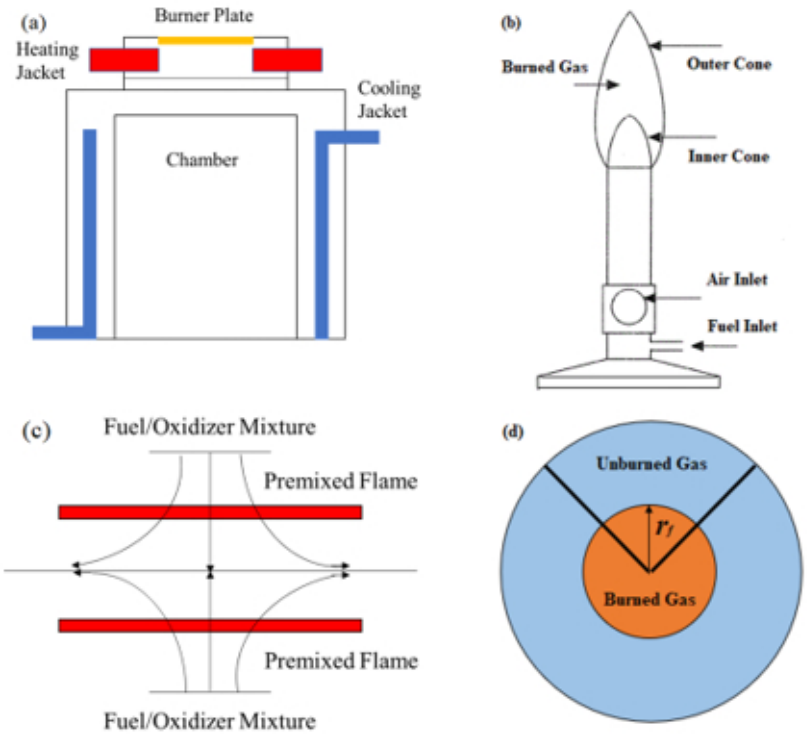


44x34mm (300 x 300 DPI)

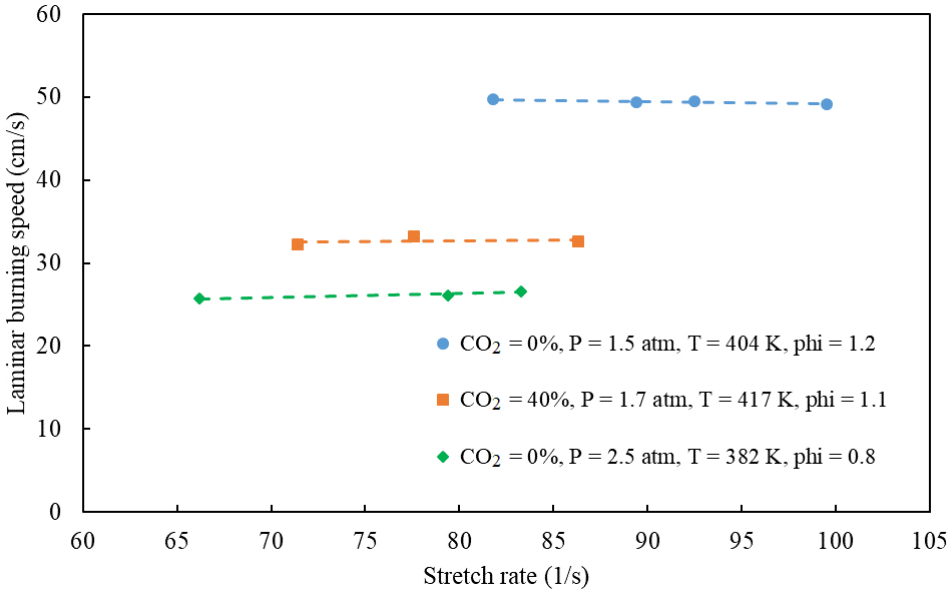


84x52mm (300 x 300 DPI)

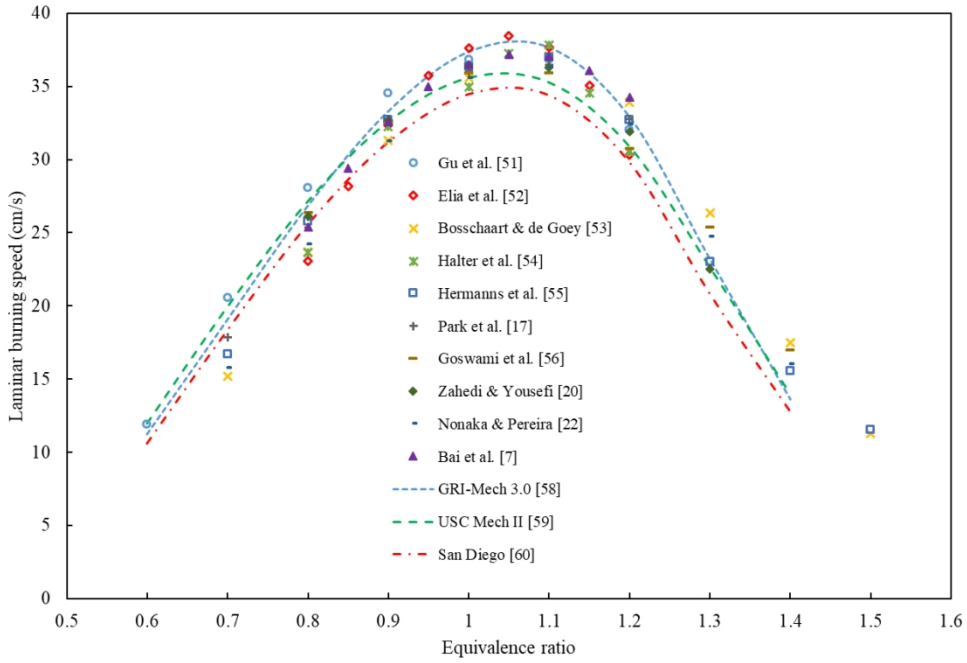


110x75mm (300 x 300 DPI)

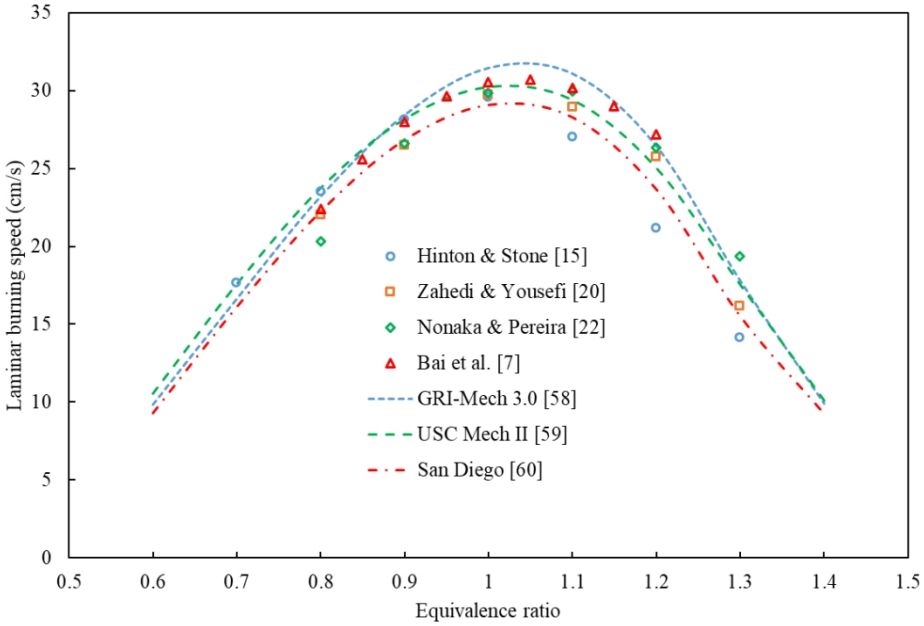


102x67mm (300 x 300 DPI)

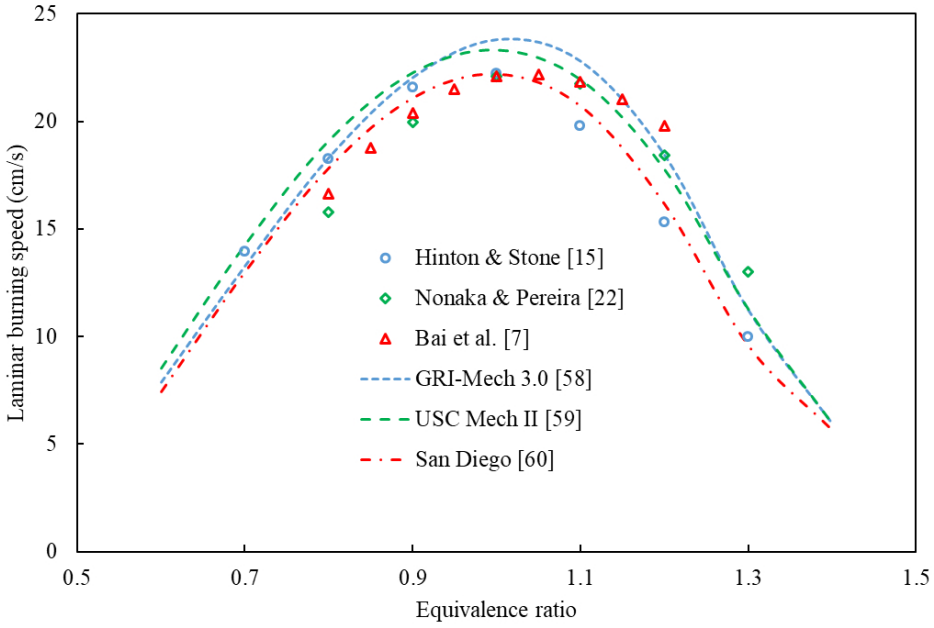


92x60mm (300 x 300 DPI)

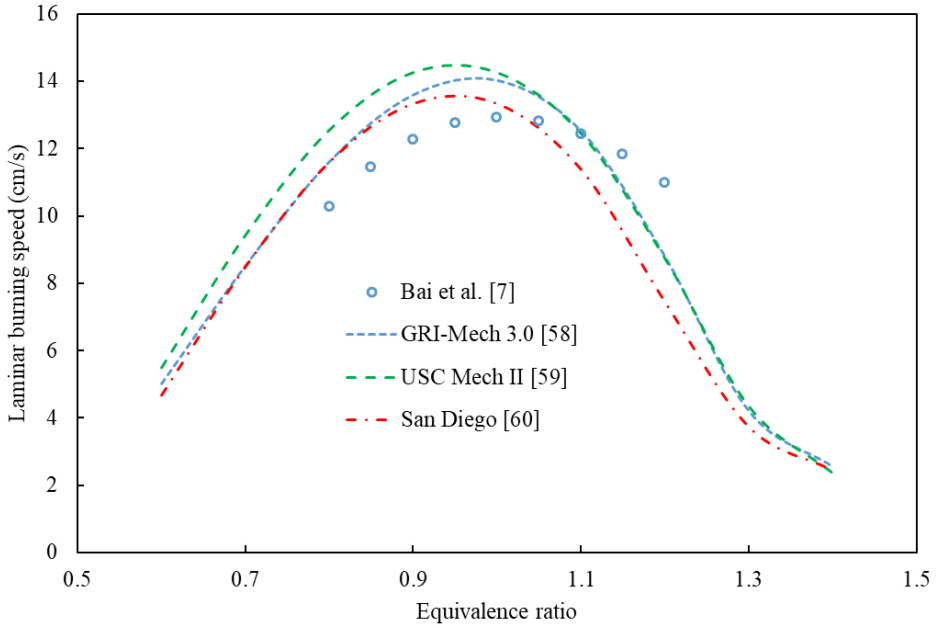


92x60mm (300 x 300 DPI)

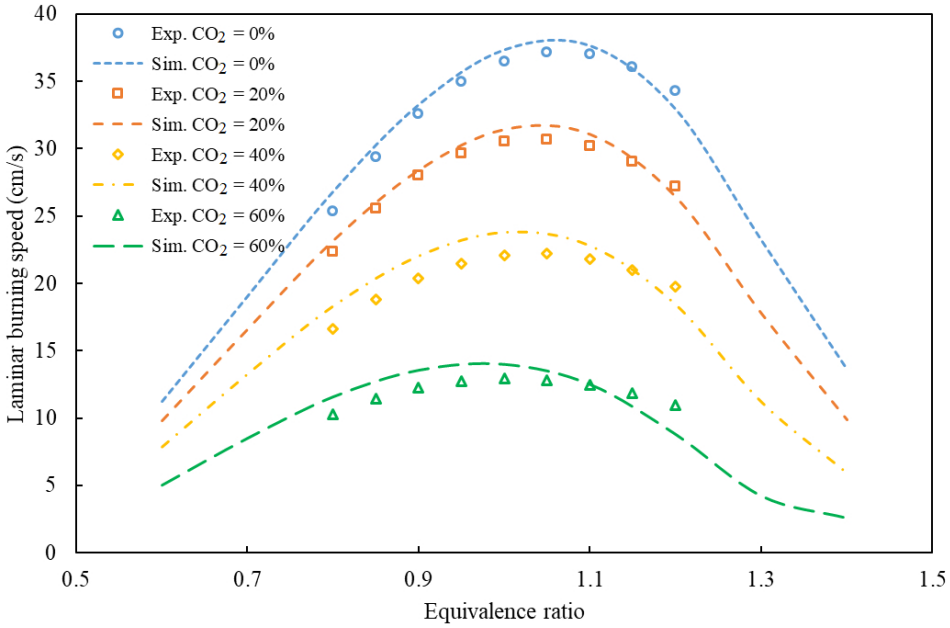


92x60mm (300 x 300 DPI)

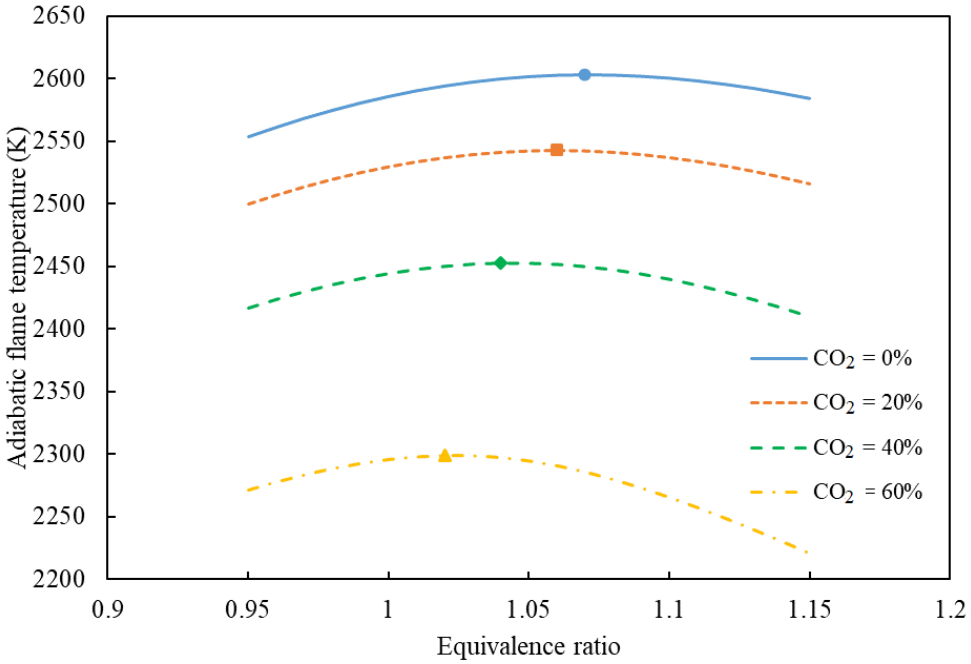


80x55mm (300 x 300 DPI)

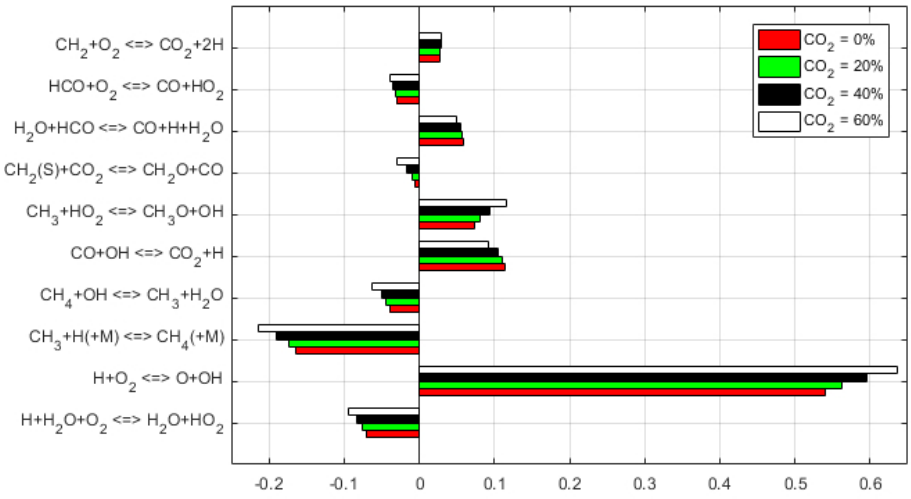


60x34mm (300 x 300 DPI)

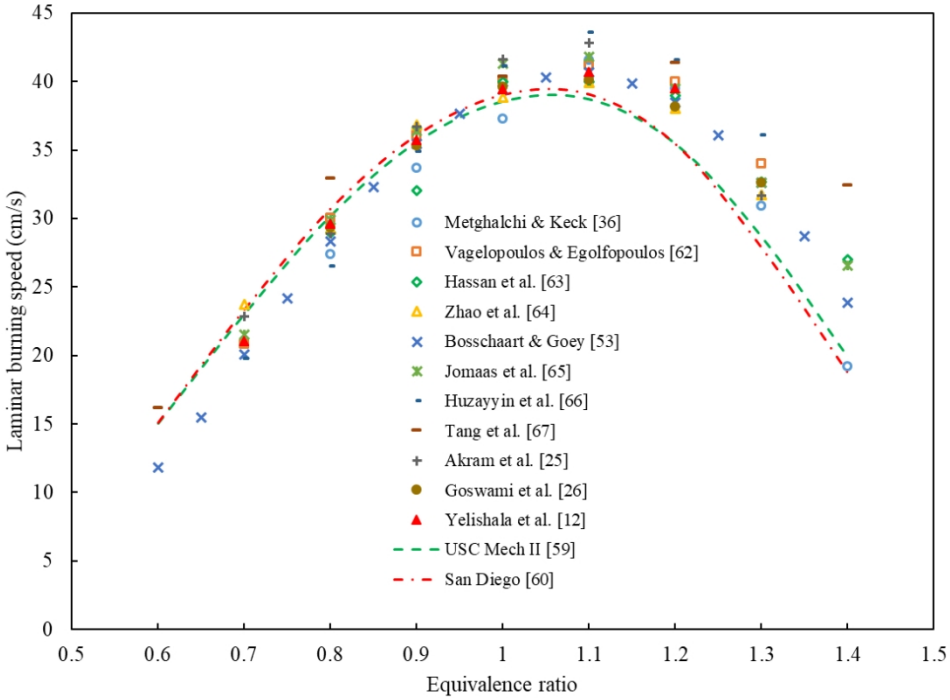


98x74mm (300 x 300 DPI)

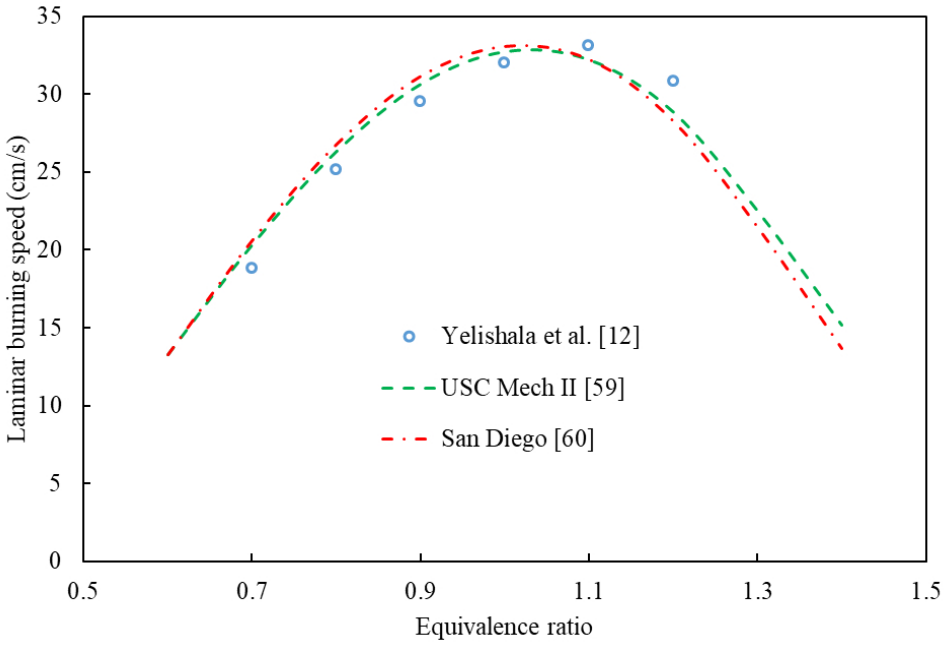


83x55mm (300 x 300 DPI)

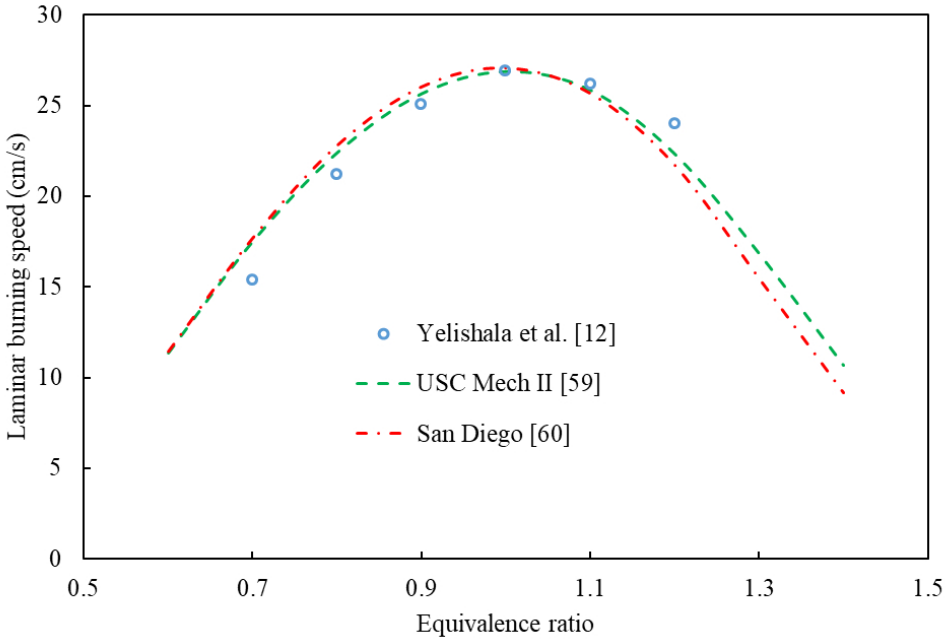


83x55mm (300 x 300 DPI)

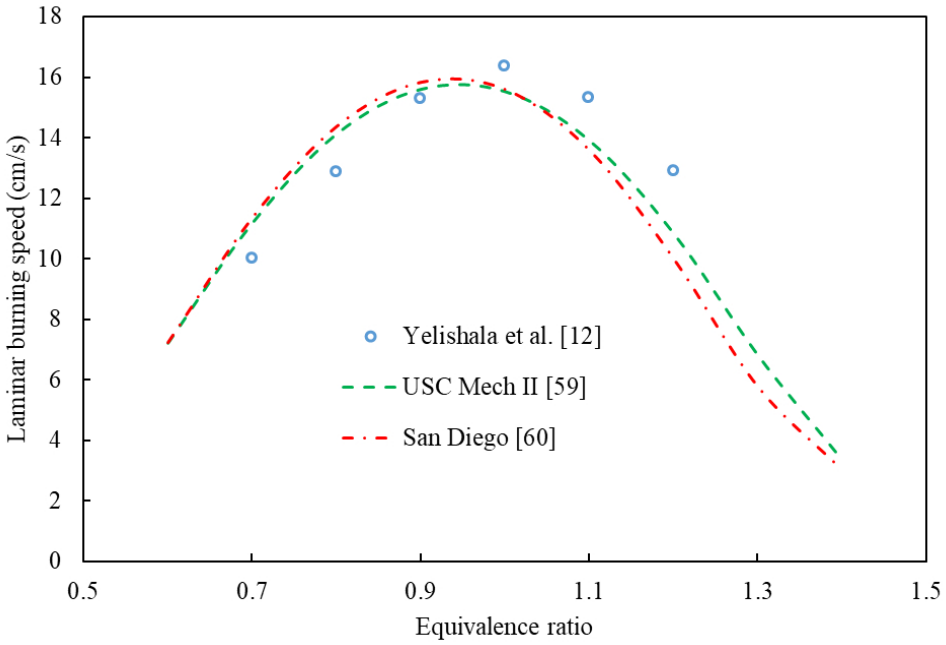


83x55mm (300 x 300 DPI)

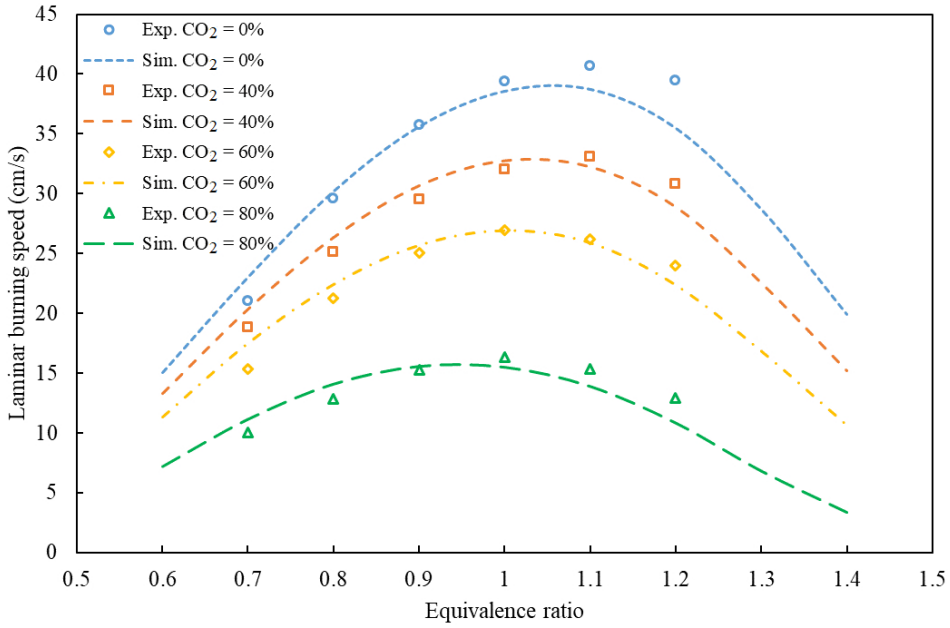


93x61mm (300 x 300 DPI)

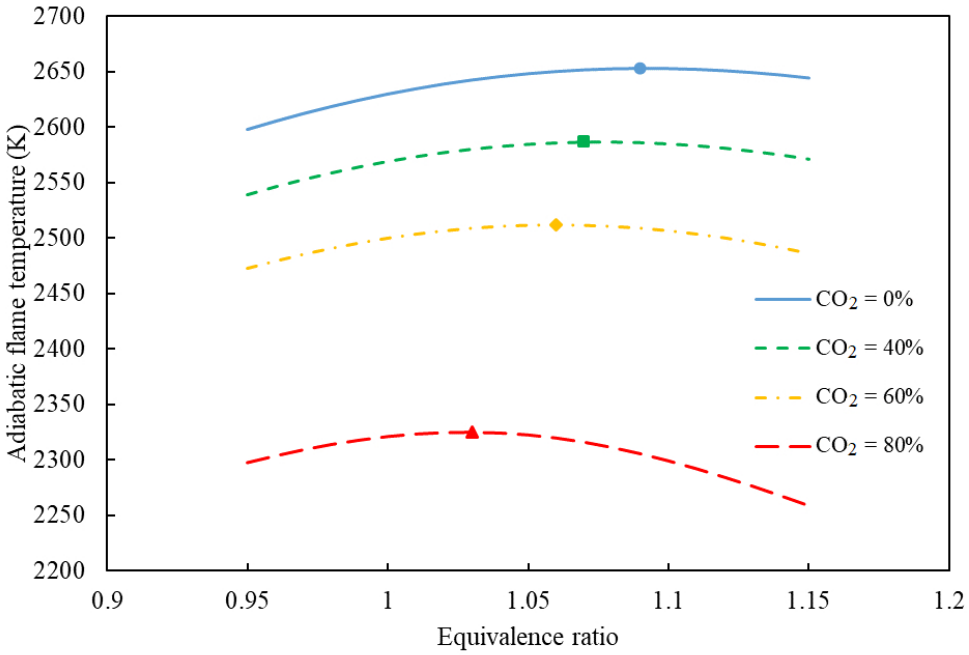


81x55mm (300 x 300 DPI)

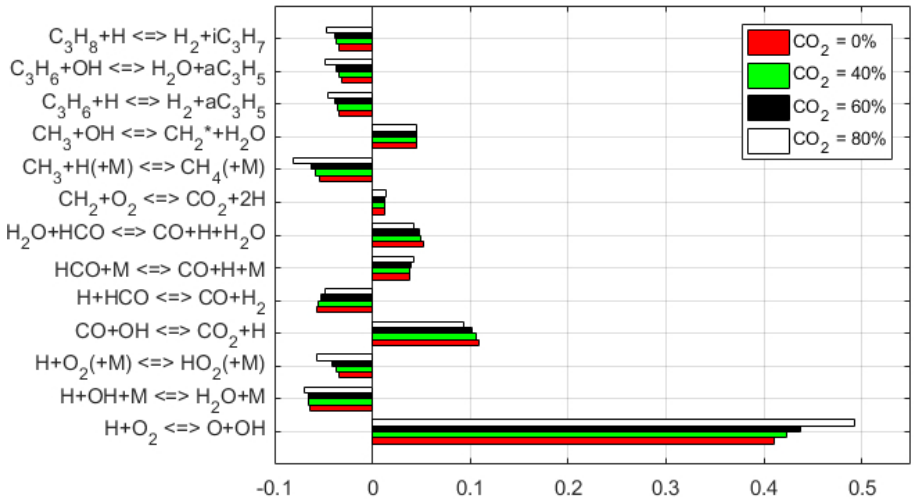


60x34mm (300 x 300 DPI)

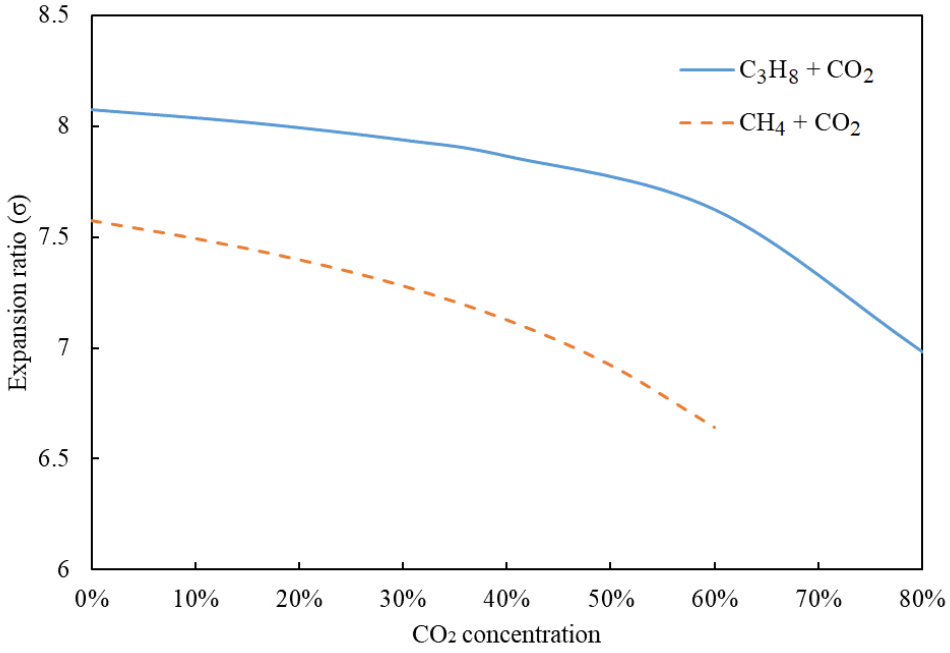


83x56mm (300 x 300 DPI)

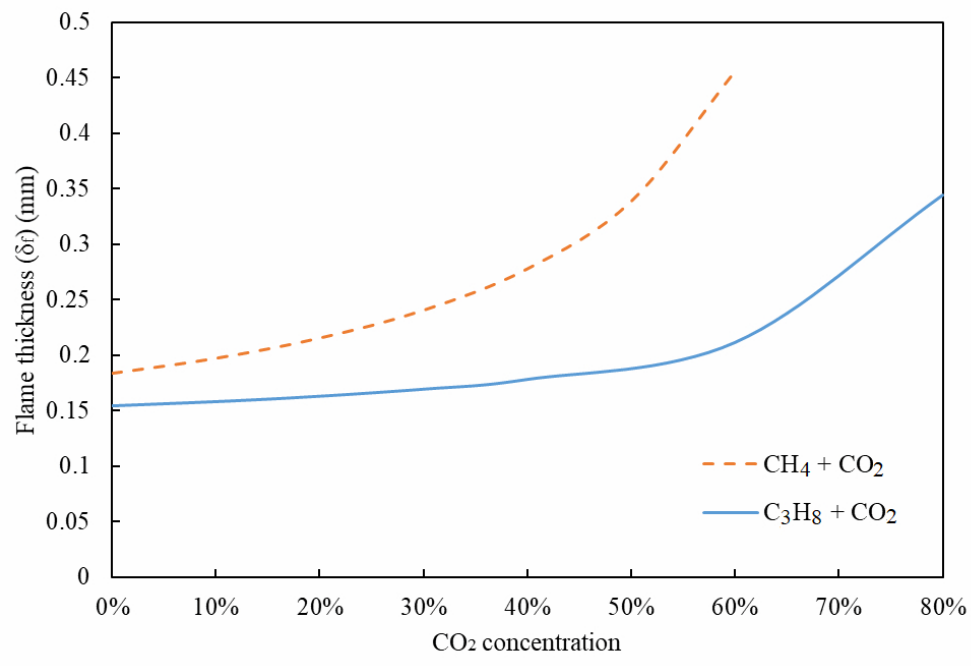


83x56mm (300 x 300 DPI)

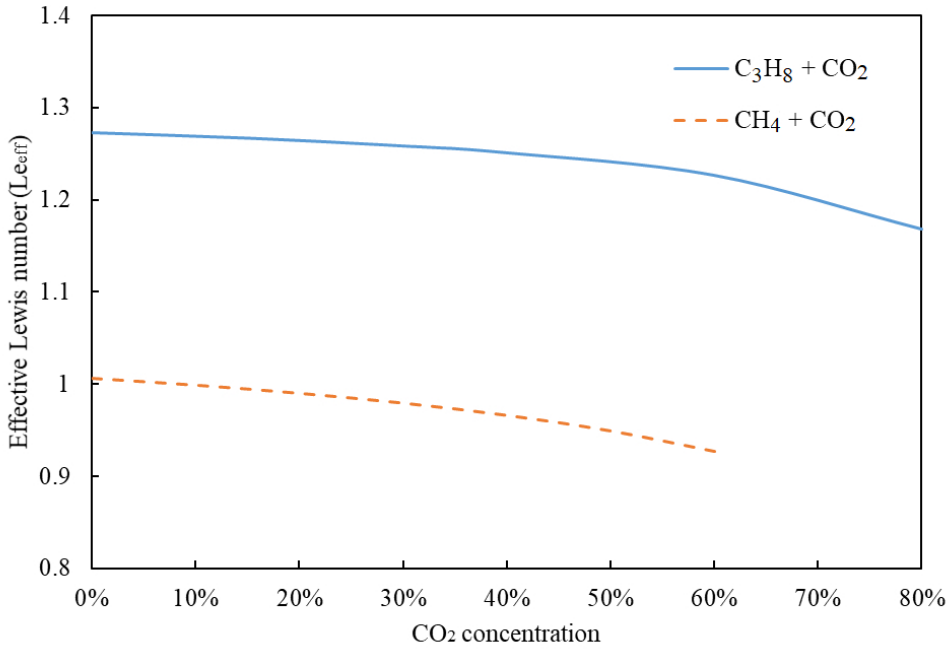


83x56mm (300 x 300 DPI)

| | 0% | 20% | 40% | 60% |
|---|---|---|---|---|
| Methane $T_i = 400\ K$ $P_i = 2.0\ atm$ $Phi = 0.8$ | 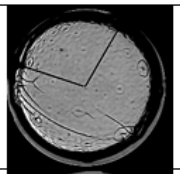 | 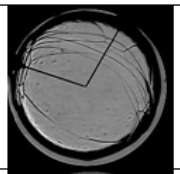 | 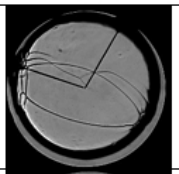 | 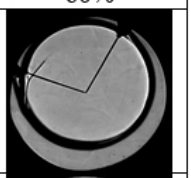 |
| Methane $T_i = 298\ K$ $P_i = 2.0\ atm$ $Phi = 1.0$ | 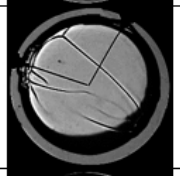 | 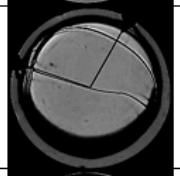 | 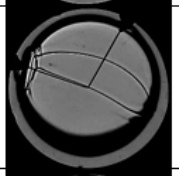 | 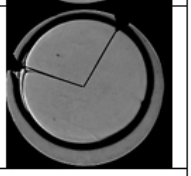 |
| Methane $T_i = 400\ K$ $P_i = 2.0\ atm$ $Phi = 1.2$ | 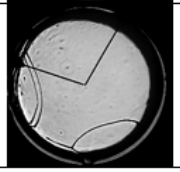 | 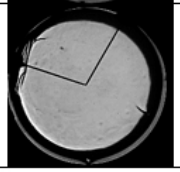 | 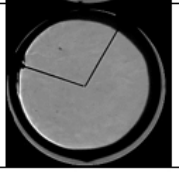 | |

59x33mm (300 x 300 DPI)